

# Specific Interactions at Cosmic Ray Energies for Extensive Air Showers Experiments\*

**V.Topor Pop<sup>1</sup>**

*Physics Department, Columbia University, New York, NY 10027*

*and*

*School of Physics and Astronomy, Tel Aviv University, Tel Aviv, Israel*

**M. Gyulassy**

*Physics Department, Columbia University, New York, NY 10027*

**H.Rebel**

*Forschungszentrum Karlsruhe, Institut fur Kernphysik III,*

*P. O. Box 3640, D-76021 Karlsruhe, Germany*

*Work submitted to Astroparticle Physics*

arXiv:nucl-th/9809014v1 4 Sep 1998

---

\*This work was supported by the Director, Office of Energy Research, Division of Nuclear Physics of the Office of High Energy and Nuclear Physics of the U. S. Department of Energy under Contract *No.DE - FG02 - 93ER40764*.

1. E-MAIL TOPOR@KAON.TAU.AC.IL; TOPOR@NT3.PHYS.COLUMBIA.EDU

The HIJING and VENUS models of relativistic hadron-nucleus and nucleus-nucleus collisions are used to study interactions of hadron-hadron, hadron-nitrogen and nucleus-nitrogen collisions, specific for the extensive air shower developments initiated by cosmic rays in the atmosphere. The transverse energy, transverse momenta and spectra of secondary particles as well as their energy and mass dependence have been investigated in detail. Results are presented with particular emphasis on the contributions of minijets in HIJING model and validity of superposition models in this energy range .

PACS : 13.85.Hd ; 13.85.Ni ; 13.85.Tp ;96.40.De;96.40.Pq;96.40.Tv

## I. INTRODUCTION

The investigation of the detailed shape of the energy spectrum and the mass composition of primary cosmic rays is currently a most active field of astrophysical research [1], [2].

Experiments on satellites or with balloon-borne detectors give information up to energies of ca.  $10^{14}$  eV [3]. Due to their limitations in size and weight they can hardly be extended beyond  $10^{15}$  eV, and indirect techniques, the observation of the particle-cascades in the atmosphere (extensive air showers: EAS), have to be invoked. The information about nature and energy of the primary particles is reflected by the shower development whose details and signatures for the primary particle depend on the high-energy nuclear interactions, governing the cascading processes. Thus the analysis requires a reliable description of these processes, formulated as a hadronic interaction model which can be used as generator of Monte-Carlo simulations of air showers. It should describe the currently available experimental information from accelerator experiments (in particular the data from the large collider facilities at CERN and Fermilab) and allow a justified extrapolation to experimentally unexplored energy regions. In the case of the EAS cascades, the quest is for the cross sections (multiparticle production, rapidity and transverse momentum distributions) for hadron-hadron, hadron-nucleus and nucleus-nucleus collisions as function of the energy (from pion production threshold up to ultrahigh energies), most importantly for the forward fragmentation region, while actually the central region of the collisions is best studied at accelerators. The fragmentation region is nevertheless also relevant for the interaction models describing the experimental observations at SPS energies and beyond [4,7], [8], [9].

There are many hadronic transport models en vogue which address this problem. They comprise versions of the Dual-Parton model (DPM) [10], Quark-Gluon String models (QGSM) [11], and models designated with the name of the code like VENUS [12], FRITIOF [13], HIJING [14]- [17], Parton Cascade Models [18], [19] and others. Some have been specifically developed as Monte-Carlo generator for air shower simulations at cosmic ray energies like DPM [20], HEMAS [21] and SYBILL [22].

Recently an exhaustive comparison of the interaction models with each other and with experimental data was performed for primary nucleons, mesons and nuclei in the energy range from  $E_{lab} = 10^{11}$  to  $10^{17}$  eV colliding with nucleons and nitrogen [23,25]. VENUS model approach [26] linked to the CORSIKA code [27] (now widely used for cosmic rays EAS simulations) has been used to scrutinize the superposition hypothesis in nucleus-nucleus collisions at ultrahigh energies. The hypothesis has been shown to be a rather good approximation, for the air shower cascade while Ranft [5], [28] using the DPMJET-II version of the DPM approach and considering the fragmentation and central regions with equal importance concluded that the superposition is a rather rough approximation of the reality. It was emphasized [23] that the comparison cannot give preference to one or another of the interaction models and the only way to decide between models is by comparing these with experimental data.

Our present work is based on the experience with HIJING and VENUS models. Systematic data [29,41] from heavy ion collisions provide new information. Both string-models have been applied to a variety of pp, pA and AA collision data (see references [9], [12], [15], [16], [42]). However, a consistent intercomparison of predictions of multiparticle production, transverse momentum and rapidity distributions at ultrahigh energies and with respect to their relevance in the EAS cascade is missing. The present paper is a first attempt of such a comparison, revealing the most salient features and differences in a selected number of cases. We introduce the presentation of numerical results with a brief reminder of the basis of the HIJING and VENUS models under consideration, stressing the different procedures in defining the interacting nucleon configurations, the quark-gluon string formation and the decay into secondary particles.

The models have been tested and compared at accelerator energies for proton-proton and nucleus-nucleus interactions and then theoretical predictions on pseudorapidity distributions of transverse energy, transverse momenta and secondary particles spectra as well as their impact parameter, energy and mass dependence are given using HIJING model for proton-proton, pion-proton, proton - Air Nucleus (p+Air) interactions between 1 TeV - 10000 TeV and for Nucleus - Air (A+Air) interactions at 17.86 TeV/Nucleon (corresponding to 1 PeV for iron (Fe) nucleus) and between 1 TeV - 10000 TeV. We set for Air nucleus, nitrogen (N) nucleus. A comparison with the results of ref. [23], [26] at the same energy using VENUS model is also done. The Feynman scaling behaviour of the model in this energy region, and effects of the multiple minijets production on charged multiplicity distributions are investigated. Finally a brief discussion on validity of superposition models, taken into consideration mean integrated values of transverse energy and spectrum weighted moments (as defined in references [43], [28]) predicted by HIJING model, is presented.

## II. OUTLINE OF THEORETICAL APPROACH

A detailed discussion of the HIJING Monte Carlo model was reported in references [14,17]. The formulation of HIJING was guided by the LUND-FRITIOF and Dual Parton Model(DPM) phenomenology for soft nucleus-nucleus reactions at intermediate energies ( $\sqrt{s} < 20 \text{ GeV}$ ) and implementation pQCD processes in the PHYTHIA model [44] for hadronic interactions.

Unlike heavy ion collisions at the existing AGS/BNL and SPS/CERN energies, most of the physical processes occurring at very early times in the violent collisions of heavy nuclei at cosmic ray energies involve hard or semihard parton scatterings which will result in enormous amount of jet production and can be described in terms of pQCD. Assuming independent production, it has been shown that the multiple minijets production is important in proton-antiproton ( $p\bar{p}$ ) interactions to account for the increase of total cross section [45] and the violation of Koba-Nielsen-Olesen (KNO) scaling of the charged multiplicity distributions [15].

In high energy heavy ion collisions, minijets have been estimated [46] to produce 50% (80%) of the transverse energy in central heavy ion collisions at RHIC (LHC) energies. Though they are not identified as single distinct jet they can led to a wide variety of correlations, between observables like multiplicity, transverse momentum, strangeness and fluctuations that compete with the expected signatures of a QGP. This have been studied in proton-proton ( $pp$ ) or antiproton-proton  $\bar{p}p$  collisions.

The HIJING model incorporate nuclear effects such as parton shadowing and jet quenching. HIJING is designed also to explore the range of possible initial conditions that may occur in nuclear collisions at Cosmic Ray and colliders (RHIC,LHC) energies.

In high energy heavy ion collisions, a dense hadronic or partonic matter must be produced in the central region. Because this matter can extend over a transverse dimension of at least  $R_A$ , jets with large  $P_T$  from hard scatterings have to traverse this hot environment. For the purpose of studying the property of the dense matter created during the nucleus-nucleus collisions, HIJING model include an option to model jet quenching in terms of a simple gluon splitting mechanism [15], [16].

The main usefulness of these schematic approaches for nuclear shadowing and jet quenching is to test the sensitivity of the final particle spectra .

The VENUS model is a "colour exchange" (CE) model , based on DPM and Gribov-Regge theory (GRT). A common feature of all Gribov - Regge models is their formulation within the framework of relativistic quantum theory . The basic exchange "particles" of high energy hadron-hadron scattering are Reggeons and Pomerons. Reggeons and Pomerons are not elementary, they are associated with complex diagrams. A Reggeon is a planar QCD diagram, a Pomeron a cylindrical QCD diagram, with the planar and cylindrical surfaces containing networks of gluons and closed quark loops. A simple model for the Pomeron is a gluon ladder.

HIJING is a minijet model which use a critical Pomeron with an intercept  $\alpha(0) = 1$ . Within such a minijet scheme, it is assumed that the rise of the cross sections with energy is totally due to to the rise of the minijet cross section .

Elastic amplitudes and hence total cross sections are calculated in VENUS model from Gribov's theory or multiple Pomeron exchanges. Eikonal form is derived in VENUS [12] . The mechanism for particle production in VENUS is colour exchange with the weight for "m" colour exchanges always being  $\sigma_m/\sigma_{in}$  where  $\sigma_m$  are topological cross sections, which correspond to cutting "m" Pomerons and  $\sigma_{in}$  is total inelastic cross section. All GR models ( VENUS, DPM, QGSM) consider colour exchange (CE) as the basic nucleon-nucleon mechanism whereas  $pQCD$  model calculate the cross sections perturbatively using  $QCD$  improved parton model.

In the VENUS model colour exchange in nondiffractive processes applies for valence quarks ( as far as available) and sea quarks. A unique feature of the VENUS procedure is the active role of antiquarks which also participate in the colour exchange (they are 8 possible diagrams) so that quarks and antiquarks are handled on equal footing. In addition the equivalence of the first CE with

all further CE's is a unique property. In all other models the first colour exchange is different to the others. VENUS is the only model which allows diquark break up, with the consequence of formation of "double strings".

The basic assumption of the model is that the projectile nucleon -whatever its status is after the first collisions - moves through the nucleus on a straight forward. Each interaction implies colour exchange and string formation. Such procedure starting from a parton level and forming hadron is referred as fragmentation or hadronization. In the VENUS model the strings are fragmented according the AMOR procedure ("area law models") ([12]) being based on relativistic classical string dynamics. "Area law models" provide a convenient gauge invariant energy and momentum string breaking procedure. Whereas AMOR allows a string to split into two substrings with arbitrary masses ( $string \rightarrow string_i + string_j$ ) the HIJING model which use JETSET algorithm requires one of the substrings to be on shell hadrons ( $string \rightarrow string_i + hadron$ ).

In both approaches the iterative procedure terminates, wherever the string masses are below a specified cut-off. Those strings are identified with stable hadrons or known resonances.

VENUS allows diquark break up, with the consequence of formation of "double strings", a non-conventional mechanism which may form when one projectile nucleons interacts with two or more target nucleons. A double string is defined as a colour singlet baryon configuration consisting of one projectile quark connected to two different valence quarks in the target via a three gluon vertex. Double strings(one forward quark linked via two normal strings to two backward quarks) do additionally fragment into leading baryons and therefore there is not a principal difference from the proton. However, there is a difference concerning hyperon production. The probability in the fragmentation region is enhanced by a factor of two relative to single string rates(double strings need two breakups to form a baryon and have therefore a double chance to produce an strange( $s$ ) - antistrange( $\bar{s}$ ) pair). In the used version(VENUS 4.12) the double string phenomenology is constrained to reproduce the inclusive  $p + A \rightarrow p + X$  data.

The HIJING model adopts a linear extrapolation of particle production dynamics from proton-proton ( $pp$ ) to nucleus-nucleus( $AA$ ) interactions, taking into account as essential ingredients the geometry of the nucleus and kinematical constraints.

Both models (VENUS and HIJING) take into account soft and hard scattering. In the HIJING the hard component is calculated from  $pQCD$  using a small-transverse momenta cut off. Minijets are accounted in VENUS model by considering soft and hard Pomerons (or equivalently soft and hard CE's);  $\omega = \omega_{soft} + \omega_{hard}$ , where  $\omega$  is the Fourier transform of the Pomeron propagator. A soft Pomeron provides the standard colour exchange; the string endpoints acquire some intrinsic transverse momenta ( $p_t$ ) of the order of few hundred MeV. For hard CE the transverse momentum  $p_t$  of the endpoints is distributed as  $(p_t^2 + m_h^2)^{-n_h}$  where  $m_h$  and  $n_h$  are energy independent parameters.

In VENUS model the  $pQCD$  results are used and the relative weight of hard and soft contributions

are determined by comparison with data .

### III. NUMERICAL RESULTS

In the following we present a series of calculated results of the models for inter-comparison. For the cosmic ray cascades in the atmosphere, first of all collisions of protons and heavier ions with  $^{14}N$  and  $^{16}O$  are important. For these cases there is a scarcity of data. However, experimental data are of much better quality in hadron-hadron and especially in proton-proton or antiproton-proton collisions which should be used to test the models.

#### A. PROTON - PROTON AND NUCLEUS-NUCLEUS INTERACTIONS AT ACCELERATOR ENERGIES

We start to present results of  $pp$  and  $p\bar{p}$  collisions . We include a comparison of hadron yields at collider energies ( $\sqrt{s} = 540 \text{ GeV}$  ) for  $\bar{p}p$  interactions, where mini-jet production plays a much more important role. From different collider experiments Alner et al. (UA5 Collaboration) [47] attempted to piece together a picture of the composition of a typical soft event at the Fermilab  $Spp\bar{p}S$  collider [48]. The measurements were made in various different kinematic regions and have been extrapolated in the full transverse momenta ( $p_T$ ) and rapidity range for comparison as described in reference [47]. The experimental data are compared to theoretical values obtained with  $HJJING^{(j)}$  in Table I. It was stressed by Ward [48] that the data show a substantial excess of photons compared to the mean value for pions  $\langle \pi^+ + \pi^- \rangle$  . It was suggested as a possible explanation of such enhancement a gluon Cerenkov radiation emission in hadronic collision [49]. Our calculations rules out such hypothesis. Taking into account decay from resonances and direct gamma production, good agreement is found within the experimental errors.

In the following plots the kinematic variable used to describe single particle properties are the transverse momentum  $p_T$  and the rapidity  $y$  defined as usual as:

$$y = \frac{1}{2} \ln \frac{E + p_3}{E - p_3} = \ln \frac{E + p_3}{m_T} \quad (1)$$

with  $E$ ,  $p_3$ , and  $m_T$  being energy, longitudinal momentum and transverse mass  $m_T = \sqrt{m_0^2 + p_T^2}$  with  $m_0$  being the particle rest mass.

The pseudorapidity  $\eta$  is used rather than the rapidity since for  $\eta$  no knowledge of particle masses is required :

$$\eta = \frac{1}{2} \ln \frac{p + p_3}{p - p_3} = -\ln \tan \frac{\theta}{2} \quad (2)$$

where  $p$  is the projectile nucleon momentum and  $\theta$  is the scattering angle. Feynman  $x_F$  variable is defined for ultrahigh energy as:

$$x_F = 2 \frac{m_T}{\sqrt{s}} \sinh(y^{cm}) \quad (3)$$

where  $y^{cm}$  and  $s$  are rapidity and total energy in center of mass frame (cms).

In Figure 1 we compare rapidity and transverse momentum distributions for strange particles in proton-proton interactions at 300 GeV given by HIJING model with experimental data [53]. The agreement is quite good. However, it will be interesting to investigate also the Feynman scaling behaviour of the model at the accelerator energies since the forward fragmentation region seems to play an important role [28], [9].

We focussed our analysis concerning particle production in nucleus - nucleus interactions at SPS energies, where the models should be better tested, mainly for interactions  $S + A$  at 200A GeV and  $Pb + Pb$  at 160A GeV.

Figure 2 shows that the hyperon production data require new mechanisms not apparent in proton-proton reactions (see Fig. 2a, Fig. 2b). Recall that VENUS has an extra degree of freedom relative to HIJING, a color rope effect, called *double string*. The factor of two enhancement of hyperon production is already needed (see dotted histogram). Adding final state interactions VENUS should describe better hyperon yields in AA and pA ( see ref. [9]) interaction ( see Fig. 2a,b,d - dashed histograms). The excess rapidity shift of the hyperons relative to non-strange baryons is also clear from Fig. 2a and Fig. 2c ,where in Fig. 2a the peaks are shifted approximately one unit of rapidity further than those calculated for protons [9]. The enhanced hyperon transport is currently not explained by any of these models.

The rapidity distributions for antiproton  $\bar{p}$  and for negative kaons  $K^-$  are represented for  $S + S$  interactions at 200A GeV in Figure 3 (Fig. 3a ( $\bar{p}$ ) and Fig. 3b ( $K^-$ )). We see that the effect of including extra degree of freedom and final state interaction is less pronounced . Therefore we give theoretical predictions for ( $\bar{p}$ ) (Fig.3c) and ( $K^-$ ) rapidity distributions (Fig.3d) for  $Pb + Pb$  interactions at 160A GeV without final state interactions in VENUS model comparing with HIJING.

We turn next to the distribution of valence baryons in  $A + A$  collisions at SPS for which data have finally become available from NA49 [30,32] and NA44 [31] and provide the most important test of the models. As noted in [8] data on nuclear stopping power in  $Pb + Pb$  collisions have been long awaited as a critical test of nuclear transport models and with ongoing search for nonlinear



dynamical phenomena in nuclear reactions. One source of nonlinear behavior may arise if a quark - gluon plasma is formed in such reactions.

Figure 4 compares the spectrum of pion and participants protons in  $S + S$  at 200 AGeV [38] and  $Pb + Pb$  reactions at 160 AGeV [30,31,32]. The various data sets from NA35 for  $S + S \rightarrow \pi^- + X$  correspond to different centrality triggers [38], with the higher one corresponding to a more severe veto trigger cut (see reference [38] for more details). We see that the negative pion rapidity densities are well accounted for by both HIJING and VENUS models. This is largely due to the fact that the pion distribution simply grows linearly with the atomic number between  $S + S$  and  $Pb + Pb$ . The centrality trigger was implemented in the above calculations via an impact parameter cut of  $b < 1$  fm.

The large central hole in the  $dN/dy$  predicted by HIJING is traced back here to the central hole in  $pp$  in FRITIOF type models. By choosing fragmentation functions that fit the  $pp$  central rapidity region better, VENUS, can avoid the strong suppression of the mid-rapidity protons of HIJING and other models using JETSET. We note that HIJING 1.3 utilizes the new particle conventions of JETSET 7.2 . In this version it is no longer possible to vary the diquark fragmentation scheme. The analysis that we have performed points to the necessity of modifying the baryon fragmentation part of HIJING, FRITIOF and DPM models.

Figures 4a,c demonstrate also the insensitivity of the pion distribution to the underlying baryon number flow. In particular, the rather large difference between the proton distribution in HIJING and VENUS in Fig. 4d is contrasted by the much more modest difference of the pion distributions in Fig. 4c. It was shown [9] that the forward energy flux is a more sensitive measure of the energy degradation difference between the models.

## B. PROTON -AIR NUCLEUS INTERACTIONS AT COSMIC RAYS ENERGIES

There are not sufficient experimental data available for the fragmentation region of hadron collisions with light target nuclei. Hence many feature for these collisions have to be inferred by studies of interaction models.

A comparative study of the predictions of different models has been done recently in ref. [23,25]. It was shown that clear differences in the results exist and that differences between models are smaller for iron primaries than for primary protons. Since consistent theoretical predictions of multiparticle production with respect to their relevance to EAS cascade is missing for HIJING , we performed such kind of analysis. Some specific interactions were investigated in HIJING approach at RICH and LHC energies [15]- [17].

We start taken into consideration some specific spectra of secondary particles analysing in detail especially transverse energy, transverse momenta or Feynman  $x_F$  distributions.

We generate for proton-Air Nucleus ( $p + Air$ ) interactions  $10^4$  minimum bias events ( $b_{min} = 0$ ,  $b_{max} = 5fm$ ). In order to give an idea about energy used for producing new particle we investigate in Figure 5 the transverse energy pseudorapidities spectra and their dependence with energy for all secondaries (Fig. 5a), all neutral (Figure 5b), all charged (Fig. 5c) and gluons (Fig. 5d). As we see from Figure 5 gluons carried an important fraction from transverse energy and this fraction increase with increasing energy (from 2.8 % at 1 TeV to 17.3 % at 1000 TeV). Also the percentage of occurrence of gluons increase from 7.20 % at 17.86 TeV to 10.71 % at 1000 TeV (see Table II).

The rapidity distributions and energy dependence of main secondary particles are shown in Figure 6 and Figure 7. Secondary  $\pi^\pm$  (Fig. 6a and 6b) and  $K^\pm$  (Fig. 6c and 6d) are the source of Cosmic Ray Muons and the source of atmospheric Neutrinos produced by the Cosmic Ray cascade. Secondary  $\pi^0$  (Fig. 7a) and  $\eta$  mesons are the source of the electromagnetic shower and secondary charmed mesons (Fig. 7d) are the source for prompt Muons and Neutrinos. The lambdas have been shown (Fig. 7c), because they can be produced from protons by exchanging a single valence quark by strange quark. The outer maximum of their distributions are due to this process. This component is identified in all nucleon distributions (neutron, proton). The statistics ( $10^4$  events generated) seems not to be enough for charmed mesons ( $D^\pm$ ) but we give such distributions only to show that introducing HIJING code in a shower code with a much higher statistics at simulation level a study of prompt muon component should be feasible.

We see from Figure 6 that mesons distributions exhibit a broad structureless shape which does not depend strongly on the type of mesons but have a dependence on energy from 1 TeV to 1000 TeV.

Trying to stress out the relevance of accelerator data on particle production in hadron - nucleus collisions for Cosmic Ray cascade we study the Feynman scaling behaviour of  $p + Air \rightarrow \pi^\pm + X$  and  $p + Air \rightarrow p + \bar{p} + X$  in Fig. 9a and Fig. 9b respectively. We plot the  $x_F dN/dx_F$  distributions for laboratory energies of 1 TeV (dotted histograms), 100 TeV (dashed histograms), 1000 TeV (solid histograms). The violations of Feynman scaling which occur are connected with known rise of rapidity plateau for all kinds of produced particles and with production of minijets. Due to minijets Feynman scaling is more strongly violated especially in the region  $x_F \geq 0$ . The violation of Feynman scaling are less dramatic in DPMJET II model [4], [5] and appear only around  $x_F = 0$  and  $x_F = 1$ . We note also that HIJING show violation of KNO scaling due to the production of multiple minijets and the tendency becomes stronger with increasing energy [15].

In order to evaluate multiplicity distributions for the charged particles in  $p + Air$  interactions (Fig. 10a) we differentiate the contributions from soft ( events with  $N_{jet} = 0$  represented in Fig. 10b) and hard processes ( events with  $N_{jet} = 1$  in Fig. 10c and for events with  $N_{jet} > 1$  in Fig. 10d) where  $N_{jet}$  is the number of minijets produced in that events. Our calculations including the effects of multiple minijets are the contributions from the events which have hard collisions with  $P_T > P_{0j}$

= 2 GeV/c. Analysing Figure 10 it is clear that the events at the tails of the charged multiplicity distributions in p+Air interactions are mainly those with multiple minijets production.

### C. NUCLEUS-NUCLEUS AIR INTERACTIONS AT COSMIC RAYS ENERGIES

Nucleus-Air collisions are of great importance in the EAS development. It is important, that the model will be able to give a good description of hadron production in nucleus-nucleus interactions. In this subsection we try to investigate mainly the dependence on projectile mass for specific interactions for EAS (He, Ne, S, Fe+Air Nucleus) at 17.86 TeV/Nucleon which correspond to 1 PeV laboratory energy for Fe nucleus.

At SPS energies the calculated number of target and projectile participants as well as the number of participants as a function of reaction impact parameter ( $b$  fm) [50] shows no difference in HIJING and VENUS model [9].

The results depicted in Figure 11 are obtained for  $10^4$  generated events and for the following intervals of impact parameter ( $b_{min} - b_{max}$ ) : Fe + Air (0-13 fm), S + Air (0-11 fm), Ne + Air (0-10 fm), He + Air (0-7 fm) - dotted histograms ; Fe + Air (0- 8 fm), S + Air (0-7 fm), Ne + Air (0-6 fm), He + Air (0-5 fm ) - dashed histograms ; Fe + Air (0 - 5 fm), S + Air (0 - 5 fm), Ne + Air (0 - 5 fm), He + Air (0-4 fm) - solid histograms.

Figure 11(a, b, c, d) shows strongly dependence on impact parameter intervals ( $b_{min}-b_{max}$ ) for theoretical predictions at 17.86 TeV/Nucleon .

Therefore for comparison of HIJING and VENUS results at 17.86 TeV/Nucleon for p+Air, He+Air, Ne+Air, S+Air, Fe+Air and for p+Air at 1000 TeV we try to get approximatively the same number of participants. For HIJING model we get the values for mean numbers of participants listed in last lines of Table II for  $10^4$  generated events and the following impact parameter intervals ( $b_{min} - b_{max}$ ): He+Air(0-4 fm), Ne+Air(0-6 fm), S+Air (0-7 fm), Fe+Air (0-8 fm) ,  $p + Air$  (0- 5 fm). The results for VENUS model are taken from Schatz et al. [26].

Table II lists the frequency of various particles among the secondaries for collisions of different nuclei with nitrogen. Our calculations confirm the results from reference [26] .The percentages do not seem to depend strongly on projectile mass nor, as shown by proton results on energy. We see only a slight tendency of increasing strangeness production with increasing primary mass for VENUS results. Analysing the results of Table II we see that the VENUS model predict more pions and kaons, but less gamma particles that HIJING model . We remark also differences in total multiplicities at ultrahigh energies which can not be explained only by the difference between total number of participants . It seems that "double string" mechanism change considerably the baryon spectra and allows the baryon number to migrate several units of rapidity from the end point rapidity.

Important for Cosmic Ray studies and EAS development is also the dependence of particle pro-

duction on the nuclear target and projectile. Taking into consideration the same conditions as those reported for the values listed in Table II the theoretical predictions for mass dependence of pseudorapidity spectra are given for transverse energy in Figure 12, for transverse momenta in Figure 13 and for main secondaries produced new particles in Figure 14. The transverse momenta distributions of all charged, proton,  $\pi^+, \pi^-$  are displayed in Figure 15 for limited interval of pseudorapidity  $|\eta| < 0.5$ .

For Feynman  $x_F dN/dx_F$  distributions we give theoretical values for specific EAS interactions in Figure 16 only for charged pions( Fig.16a) and for protons(Fig.16b). We see a slight mass dependence of Feynman distributions and transverse momenta distributions for  $A \geq 20$  (Fig.15a-d).

Instead of the proper sampling of Nucleus + Air Nucleus scattering events, an approximation often applied in EAS development is the so called superposition model. There are two different possible superposition models: a nucleus-nucleus collision A-B with  $N_{part}$  participating nucleons is approximated as the superposition of  $N_{part}$  simultaneous nucleon-nucleon collisions and the second one : a nucleus-nucleus collision A-B with  $N_{proj}$  participating projectile nucleons is approximated as the superposition of  $N_{proj}$  simultaneous nucleon-B collisions. The validity of this principle was analysed in some recent works [26], [4], [5], [28] and older one [51], [52] with different conclusions.

In this section we investigate using HIJING approach the integrated mean transverse energy for secondaries produced in Nucleus+Air Nucleus interactions at 17.86 TeV/Nucleon. So, we generate  $10^4$  events in the same impact parameter interval (0-5 fm) for Fe, S, Ne, He, p+Air interactions. The values obtained for mean projectile participants ( $N_{proj}$ ) and mean number of binary collisions  $N_{coll}$ (which include nucleon-nucleon( $N - N$ ), nucleon-wounded nucleon( $N - N_w$ ), wounded nucleon-nucleon  $N_w - N$  and wounded nucleon-wounded nucleon  $N_w - N_w$  collisions) are listed in Table III. The results given in Table III are for all secondaries , all charged and all neutrals particles produced in interactions. The values of integrated mean transverse energy  $\langle E_T \rangle$  scale with the number of binary collisions in nucleus-nucleus interactions at this energy  $N_{coll}$  and scaling properties are valid for  $A \geq 20$  and should not be applied to light nucleus+Air interactions. Since integrated mean value of transverse energy  $\langle E_T \rangle$  is a measurable quantity it will be interesting to verify this scaling at RHIC and LHC energies.

In order to evaluate multiplicity distributions for charged particles in A + Air interactions we differentiate the contribution for all events (soft + hard) (Fig. 17a for Fe + Air and Fig. 17b for S + Air ) and only hard processes - events with  $N_{jet} > 1$  (Fig. 17c for Fe + Air and Fig. 17d for S + Air ). We can see from Figure 17 that the low multiplicity events are dominated by those of no jet production while high multiplicity events are dominated by those of at least one jet production. Also it is clear from Figure 17 that the contributions from the events which have hard collisions increase with increasing of available energy and of projectile mass.

At ultrahigh energies nuclear effects like nuclear shadowing of partons and jet quenching (see section 2), should have important contributions [15], [16]. In HIJING model a simple parametrization

of gluon shadowing and a schematic quenching model were introduced to test the sensitivity of the final distributions to these aspects of nuclear dynamics. Trying to estimate the results with and without such effects we investigate the differences for more central Fe + Air interactions at fixed energy 17.86 TeV/Nucleon. Our calculations seems to indicate for main secondary particles produced in EAS specific interactions in this energy region, that the effects should be neglected (they are less than 2 -3 %).

## IV. MORE SPECIFIC SPECTRA AT COSMIC RAY ENERGIES

### A. Feynman scaling

Since experimental data in the projectile fragmentation region are of much better quality in hadron-hadron collisions, we study the Feynman scaling behaviour of the model for energy range well below 1 TeV. In Fig. 18a a one compare results for  $\pi^-$  production in the forward and backward fragmentation regions for proton - proton interactions at 250 GeV [54] and find a reasonable agreement. In Fig. 18b the theoretical predictions are compared with experimental data from Bailly et al. [55] at 360 GeV (Fig. 18b) for  $\pi^-$  and from Aguilar-Benitez et al. [56] at 400 GeV for  $K^+$  (Fig. 20c). In Fig. 18d the data for  $\pi^+$  production at 205 GeV [57] are also compared with HIJING model prediction. All sets of data strongly disagree with the model predictions. Furthermore , the data of Aguilar-Benitez et al. [56] shows a strange structure at  $0.5 \leq x_F \leq 0.8$  which is not found in other experiments and in the model [4], [5]. We note that the model is well below the data for  $p + p \rightarrow K^+ + X$  and for  $p + p \rightarrow \pi^+ + X$ .

In Figs. 19a,b we compare  $x_F d\sigma/dx_F$  distributions for  $\Lambda$  hyperons and neutral mesons  $K_s^0$  with the experimental data of Bailly et al., at 360 GeV [55,55] . The agreement of model and data are quite good for  $K_s^0$  , but theoretical predictions overestimate the data for  $\Lambda$  in the projectile fragmentation region . Also shown dependence on energy for  $p + p \rightarrow \Lambda^0 + X$  (Fig. 19c) and  $p + p \rightarrow \gamma + X$  (Fig. 19d) between 1 TeV - 1000 TeV.

In the cosmic ray cascade the interactions of secondary hadrons mainly pions and kaons are as important as interactions of nucleons.

In Figs. 20a-d we compare the model predictions with the results of the EHS-NA22 experiment [54] in  $\pi^+ + p$  collisions at 250 GeV for  $pi^-$  (Fig. 20a) and  $h^+$  (Fig. 20c ) and with the data of Brenner et al., at 175 GeV [58] for  $\pi^+$  (Fig. 20b) and for  $pi^-$  (Fig. 20d) . These comparisons shows only partial agreement with the data, especially in central region.

## B. Comparison of nucleus - nucleus collisions according to HIJING model with superposition model

In section IIIC we have investigated the superposition model for transverse energy. In this section we will extend the energy region and also we will investigate inelasticities and spectrum-weighted moments calculated using HIJING model for C-Air collisions. The spectrum-weighted moments are defined as in Ranft et al. [28]. We introduce new variables  $x_{pL} = p_L^i/P_0$  or  $x_E = E_i/E_0$  in the laboratory frame following the basic discussion of ref. [43].  $E_i$  ( $p_L^i$ ) is the laboratory energy (momenta) of secondary particle  $i$  and  $E_0$  ( $P_0$ ) is the laboratory energy (momenta) of the projectile in hadron-nucleus collisions, or the energy per nucleon in nucleus-nucleus collisions. These variables are similarly to Feynman  $x_F$ , but expressed in the laboratory frame. We can consider  $x_E$  distributions  $F(x_E) = x_E \frac{dN_i}{dx_E}$ . The cosmic ray spectrum weighted moments in nucleus-nucleus collisions are defined as moments of the  $F(x_E)$ , taking into account the power of the integral cosmic ray energy spectrum ( $\gamma \simeq 1.7$ ):

$$Z_i = \int_0^{A_A} (x_E)^{\gamma-1} F_i(x_E) dx_E \quad (4)$$

where  $A_A$  is the mass number of the projectile nucleus  $A$ .

Table IV and V compare multiplicities and spectrum-weighted moments calculated using HIJING model for C - Air collisions. The comparisons in these two tables with both version of the superposition model show, that the superposition is a very rough and unreliable approximation to real nucleus - nucleus collisions.

In Table VI the inelasticities  $K_h$  in proton - Air collisions calculated from HIJING model are given for the most important secondaries as function of energy. Inelasticities are defined in our calculations as the fraction of the laboratory energy carried away in the average by secondary hadron of kind  $h$ . From Table VI we see that all values for inelasticities decrease with increasing energies.

In Table VII we give the spectrum weighted moments for pion and kaon production.  $Z_\pi$  and  $Z_K$  obtained in HIJING model for  $pN$  collisions in comparison with the values predicted by others model: DPMJET [4], [5] HEMAS [21] and SIBYLL [22]. We see that the values in HIJING models have a weak dependence on energy from 1 TeV up to 10000 TeV and the moments for  $p + N$  collisions are smaller than in  $p + p$  collisions. We mention that the same result have been obtained in DPM approach by Ranft [4], [5].

## V. CONCLUSIONS

In this paper an analysis of particle production is performed for hadron-hadron, hadron-nitrogen and nucleus-nitrogen collisions, specific for EAS developments initiated by cosmic rays in the atmosphere. The models HIJING and VENUS have been used for guidance in understanding of primary interactions. They are compared with the results at accelerator energies, in cases where experimental data exist.

A very good agreement is found within experimental errors for ultrahigh energies ( $\sqrt{s} = 540 \text{ GeV}$ ) in HIJING approach where mini-jet production plays a much more important role. For nucleus-nucleus collisions at SPS energies the rapidity spectra are well accounted for both HIJING and VENUS models for mesons, but VENUS model seems to give a better description for hyperons production. By choosing fragmentation functions that fit the  $pp$  central rapidity region better, VENUS, can avoid the strong suppression of the mid-rapidity protons of HIJING model. The analysis that we have performed points to the necessity of modifying the baryon fragmentation part of HIJING model. At SPS energies a final state interactions in dense matter as well as a color rope effect predicts much higher degree of baryon stopping at midrapidity than HIJING.

The event generator VENUS [23], [26] and HIJING in the present study were tested to simulate ultrahigh energy collisions for hadron-Nitrogen and Nucleus-Nitrogen interactions. The transverse energy, transverse momenta and secondary particles produced spectra, inelasticities, spectrum weighted moments  $Z_h$ , as well as their energy and mass dependences have been investigated in detail. The theoretical predictions for HIJING model suggest a scaling with number of binary nucleon-nucleon collisions for mean transverse energy of secondaries. It will be interesting to verify this hypothesis at RHIC energies and LHC energies.

The contributions from the events which have hard collisions are strongly evidenced at the tail of charged particles multiplicity distributions and increase with increasing energy and increasing mass of projectile.

At accelerator energies HIJING model gives only partial description of experimental data for Feynman distributions and fails to reproduce the fragmentation regions. Feynman scaling is more strongly violated in HIJING model due to multiple minijets events, especially in the projectile fragmentation region. For Cosmic Ray energies and specific EAS interactions effects of parton shadowing and jet quenching could be neglected.

Possible utilization inside a shower code of these models allows to extend the analysis and to release the simple superposition model which seems to be partially not satisfied in this energy interval.

## VI. ACKNOWLEDGEMENTS

We are grateful to K. Werner for providing us the source code of VENUS. One of the authors (VTP) would like to express his gratitude to M. Morando and R. A. Ricci for kind hospitality and acknowledge financial support from INFN-Sezione di Padova, Italy where part of the presented calculations have been performed.

---

- [1] Proceedings of the 9th International Symposium On Very High Cosmic Ray Interactions, Karlsruhe, Germany, 19-23 August 1996, edited by H. Rebel, G. Schatz and J. Knapp, Nucl. Phys. (Proceedings Supplement) **52B** (1997), p.1-298
- [2] H. Rebel in *Topics in Atomic and Nuclear Collisions* (NATO ASI Series **B321**, edited by B. Remaud , A. Calboreanu and V. Zoran (New Plenum), p397, (1994)
- [3] D. Muller, S. P. Swordy, P. Meyer, L. Heures and J. M. Grunsfeld , *Astrophys. J.* **374** , 356 (1991);  
S. P. Swordy, L. Heures, P. Meyer and D. Muller, *Astrophys. J.* **403**, 658 (1993)
- [4] J. Ranft, *Phys. Rev.* **D51**, 64 (1995)
- [5] G. Battistoni, C. Forti, J. Ranft, *Astroparticle Physics* **3**, 157 (1995)
- [6] A. Ferrari, P. R. Sala, J. Ranft and S. Roesler, *Z. Phys.* **C70**, 413 (1996)
- [7] A. Ferrari, P. R. Sala, J. Ranft and S. Roesler, *Z. Phys.* **C71**, 75 (1996)
- [8] M. Gyulassy in Proc. of Eleventh International Conference on Ultrarelativistic Nucleus-Nucleus Collisions, Quark Matter '95 (Monterey,California,USA 9-13 January,1995), edited by A.M. Poskanzer, J.W. Harris and L.S. Schroder *Nucl. Phys.* **A590** , 431c (1995)
- [9] M. Gyulassy, V. Topor Pop, S. E. Vance , *Heavy Ion Physics*, **5**, 299 (1997)
- [10] A. Capella, U. Sukhatme, C. I. Tan and J. Tran Thanh Van , *Phys. Rep.* **236**, 225 (1994)
- [11] N. S. Amelin , E. F. Staubo, L. P. Csernai, V. D. Toneev, K. K. Gudima,



- Phys. Rev. **C44**, 1541 (1991) ;
- N. S. Amelin, L. V. Bravina, L. P. Csernai, V. D. Toneev K. K. Gudima, S. Yu. Sivoklokov, Phys. Rev. **C47**, 2299 (1993)
- [12] K. Werner, Phys. Rep. **232**, 87 (1993)
- [13] B. Andersson, G. Gustafson and B. Nilsson- Almqvist Nucl. Phys. **B281**, 289 (1987);  
B. Nilsson-Almqvist and E. Stenlund, Comp. Phys. Commun. **43**, 387 (1987)
- [14] Xin-Nian Wang and Miklos Gyulassy, Comp. Phys. Comm. **83**, 307 (1994)
- [15] Xin-Nian Wang, Phys. Rev. **D43**, 104 (1991)
- [16] Xin-Nian Wang and Miklos Gyulassy, Phys. Rev. **D44**, 3501 (1991)
- [17] Xin-Nian Wang and Miklos Gyulassy, Phys. Rev. **D45**, 844 (1992)
- [18] K. Geiger, Phys. Rep. **258**, 237 (1995)
- [19] N. S. Amelin, H. Stocker, W. Greiner, N. Armesto,  
M. A. Braun and C. Pajares, Phys. Rev. **C52**, 362 (1995)
- [20] J. N. Capdevielle , J. Phys. **G** : Nucl. Phys. **15**, 909 (1989)
- [21] C. Forti, H. Biloken, B. Piazzoli, T. K. Gaisser, L. Satta and T. Stanev, Phys. Rev. **D42**, 3668 (1990)
- [22] R. S. Fletcher, T. K. Gaisser, P. Lipari and T. Stanev, Phys. Rev. **D50**, 5710 (1994)
- [23] J. Knapp, D. Heck, G. Schatz, FZKA -Report **5828**, Forschungszentrum Karlsruhe GmbH, Karlsruhe (1996)
- [24] J. Knapp, D. Heck, G. Schatz , Nucl. Phys. **52B**, 136 (1997)
- [25] D. Heck, J. Knapp, G. Schatz, Nucl. Phys. **52B** 139 (1997)
- [26] G. Schatz, T. Thouw, K. Werner, J. Oehlschlager and K. Bekk , J. Phys. **G**:  
Nucl. Part. Phys. **20**, 1267 (1994)

- [27] J. N. Capdevielle et al., KFK Report **4998**, Kernforschungszentrum Karlsruhe (1992)
- [28] G. Battistoni, C. Forti, J. Ranft, S. Roesler, Preprint US-FT-/29-96 ( hep-ph/9606485)
- [29] D. Röhrich et al., Proceedings of the Conference on Strangeness in Hadronic Matter, 15 - 17 May 1996, Budapest, Hungary ( edited by T.Csörgó, P.Lévai, J. Zimányi ), APH N.S., Heavy Ion Physics **4**, 71 (1996)
- [30] T. Wienold et al., Proceedings of the Twelfth International Conference on Ultra-Relativistic Nucleus-Nucleus Collisions, Heidelberg, Germany, 20 -24 May, 1996 (edited by P. Braun Munzinger, R. Stock, H. Stöcker), Nucl. Phys. **A610**, 76c (1996)
- [31] N. Xu et al., Nucl. Phys. **A610**, 175c (1996) ; J. Bearden et al., Phys. Lett. **B372**, 339 (1996)
- [32] M. Gazdzicki et al., Nucl. Phys. **A590**, 197c (1995)
- [33] A. Bamberger et al., Z. Phys. **C43**, 25 (1989)
- [34] J. W. Harris, Proceedings of the 12 th Winter Workshop on Nuclear Dynamics, Snowbird, Utah (1995) ; John W. Harris, Berndt Muller, DUKE-TH-96-105, Ann. Rev. Nucl. Part. Sci 46 (1997) 71-107. e-Print Archive : hep-ph/9602235.
- [35] J. Bächler et al., Z. fur Phys. **C52**, 239 (1991)
- [36] S. Margetis et al., Nucl. Phys. **A590**, 355c (1995)
- [37] T. Alber et al., Phys. Rev. Lett. **75**, 3814 (1995).
- [38] J. Bächler et al., Phys. Rev. Lett. **72**, 1419 (1994).
- [39] T. Alber et. al.,Z. Phys. **C64**, 195 (1994).
- [40] T.Alber et al., Phys. Lett. **B366**, 56 (1996).
- [41] S. Margetis et al., Heavy Ion Physics **4**, 63 (1996)
- [42] V. Topor Pop, M. Gyulassy, X. N. Wang, A. Andrighetto, M. Morando, F. Pellegrini,

- R. A. Ricci, G. Segato, Phys. Rev. **C52**, 1618 (1995) ; M. Gyulassy, V. Topor Pop, X. N. Wang, Phys. Rev. **C54**, 1496 (1996)
- [43] T. K. Gaisser, *Cosmic Rays and Particle Physics*, Cambridge University Press, 1990
- [44] T. Sjostrand, Comp. Phys. Comm. **82**, 74 (1994)
- [45] A. Capella and J. Tran Thanh Van, Z. Phys. **C 23**, 165 (1984); T. K. Gaisser and F. Halzen, Phys. Rev. Lett. **54**, 1754 (1985)
- [46] K. J. Eskola, K. Kajantie and J. Lindfors, Nucl. Phys. **B323**, 37 (1989)
- [47] G. J. Alner et al., Phys. Rep. **154**, 247 (1987)
- [48] D. R. Ward *Properties of Soft Proton Antiproton Collisions* in Advances Series on Direction in High Energy Physics, Vol. 4, Edited by G. Altarelli and L. Di Lella, 1989 , p.85
- [49] I. M. Dremin , Sov. J. Nucl. Phys. **33**, 726 (1981)
- [50] T. C. Awes, S. P. Sorensen , Nucl. Phys. **A498**, 123c (1989).
- [51] N. N. Kalmykov and S. S. Ostapchencko , Sov. J. Nucl. Phys. **50** ,315 (1989)
- [52] N. N. Kalmykov and S. S. Ostapchencko , Sov. J. Nucl. Phys. **56** , 105 (1993)
- [53] F. Lo Pinto et al., Phys. Rev. **D22**, 573 (1980)
- [54] EHS - NA 22 Collaboration, M. Adamus et al., Z. Phys. **C39** 311 (1988)
- [55] EHS-RCBC Collaboration, Z. Physik , **C35**, 309 (1987)
- [56] LEBS-EHS Collaboration , Z. Physik , **C50**, 405 (1991)
- [57] T. Kafka et al., Phys. Rev. **D16**, 1261 (1977)
- [58] A. E. Brenner et al. , Phys. Rev. **D26**, 1497 (1982)
- [59] J. L. Bailly et al., Z. Physik , **C31**, 367 (1986)

TABLE I. Particle composition of  $p + \bar{p}$  interactions at 540 GeV in cms.

Particle type	$\langle n \rangle$	Exp.data	HIJING <sup>(j)</sup>
All charged	$29.4 \pm 0.3$	[47]	28.2
$K^0 + \bar{K}^0$	$2.24 \pm 0.16$	[47]	1.98
$K^+ + K^-$	$2.24 \pm 0.16$	[47]	2.06
$p + \bar{p}$	$1.45 \pm 0.15$	[48]	1.55
$\Lambda + \bar{\Lambda}$	$0.53 \pm 0.11$	[47]	0.50
$\Sigma^+ + \Sigma^- + \bar{\Sigma}^+ + \bar{\Sigma}^-$	$0.27 \pm 0.06$	[48]	0.23
$\Xi^-$	$0.04 \pm 0.01$	[47]	0.037
$\gamma$	$33 \pm 3$	[47]	29.02
$\pi^+ + \pi^-$	$23.9 \pm 0.4$	[47]	23.29
$K_s^0$	$1.1 \pm 0.1$	[47]	0.99
$\pi^0$	$11.0 \pm 0.4$	[48]	13.36

TABLE II. Percentage of occurrence of various particles among the secondaries of a Nucleus-Air collision as calculated by the HIJING and VENUS models. The number of protons and neutrons have been reduced by respective numbers in the primary system (values labeled by star(\*) [26]). The average multiplicity and the numbers of participants are also given.

Particle type	Projectile Energy (TeV/N)	<sup>56</sup> Fe	<sup>32</sup> S	<sup>20</sup> Ne	<sup>4</sup> He	p	p
		17.86	17.86	17.86	17.86	17.86	1000
$\langle \pi^- + \pi^+ \rangle$	HIJING	45.98	45.93	45.96	45.86	45.76	46.57
	VENUS	51.02	51.29	51.48	52.34	53.05	52.15
$\langle \pi^0 \rangle$	HIJING	26.13	26.02	26.10	25.93	26.04	26.38
	VENUS	28.30	28.52	28.49	28.85	28.93	28.43
$\langle K^+ + K^- \rangle$ K mesons	HIJING	5.20	5.20	5.20	5.20	5.16	5.58
	VENUS	12.35	12.02	11.84	11.11	10.51	10.86
$\langle K_s^0 \rangle$	HIJING	2.54	2.57	2.53	2.52	2.57	2.75
$\langle p \rangle$	HIJING	4.16	4.20	4.20	4.37	4.78	3.25
$\langle p \rangle *$	VENUS	0.70	0.66	0.66	0.66	-0.11	0.66
$\langle n \rangle$	HIJING	4.12	4.20	4.23	4.40	4.16	2.86
$\langle n \rangle *$	VENUS	0.54	0.61	0.64	0.66	1.49	1.43
$\langle \Lambda \rangle$	HIJING	0.70	0.70	0.71	0.72	0.72	0.56
$\langle \Lambda + \Sigma^0 \rangle$	VENUS	1.66	1.64	1.67	1.60	1.55	1.31
$\langle \gamma \rangle$	HIJING	4.30	4.30	4.33	4.23	4.27	4.48
	VENUS	1.60	1.48	1.43	1.20	1.12	1.18
all charged	HIJING	57.30	57.47	57.54	57.54	57.84	57.79
all neutrals	HIJING	42.33	42.57	42.61	42.50	42.40	42.18
$\langle \bar{p} \rangle$	HIJING	1.42	1.38	1.43	1.40	1.41	1.56
$\langle \bar{n} \rangle$	HIJING	1.40	1.38	1.43	1.40	1.41	1.60
$\langle q + \bar{q} \rangle$	HIJING	0.40	0.43	0.41	0.36	0.33	0.71
Mean	HIJING	274.0	217.5	203.0	88.7	38.9	51.7

<b>multiplicity</b>	<b>VENUS</b>	354.7	270.5	209.3	92.6	49.4	106.5
<b>Mean projectile</b>	<b>HIJING</b>	9.6	7.2	6.5	2.2	1.0	1.0
<b>participants</b>	<b>VENUS</b>	12.1	8.1	5.7	2.1	1.0	1.0
<b>Mean target</b>	<b>HIJING</b>	5.9	5.6	5.6	3.4	2.06	1.42
<b>participants</b>	<b>VENUS</b>	6.0	5.3	4.7	3.2	2.0	2.06

TABLE III. Mean transverse energy for the secondaries of a Nucleus-Air collisions at 17.86 TeV/Nucleon as calculated by the HIJING model and by considering superposition of  $N_{coll}$  nucleon-nucleus collisions and  $N_{proj}$  nucleon-nucleus collisions, where  $N_{coll}$  is the number of binary collisions and  $N_{proj}$  is the number of participant projectile nucleons.  $E_T^{pA}$  is mean transverse energy in p+Air interaction at the same energy and in the same impact parameter interval (see the text for explanation).

	<b>Projectile</b>	<b><math>^{56}\text{Fe}</math></b>	<b><math>^{32}\text{S}</math></b>	<b><math>^{20}\text{Ne}</math></b>	<b><math>^4\text{He}</math></b>	<b>p</b>
<b>Mean number</b>	$\langle N_{coll} \rangle$	27.75	19.21	13.61	2.62	
<b>Mean number</b>	$\langle N_{proj} \rangle$	18.43	11.44	8.24	1.73	
<b>Mean Transverse</b>	<b>all secondaries</b>	212.5	140.7	104.2	25.16	7.54
<b>Energy</b>	$N_{coll} * E_T^{pA}$	209.2	144.8	102.6	19.75	
<b>(GeV)</b>	$N_{proj} * E_T^{pA}$	138.96	86.25	62.10	13.04	
<b>Mean Transverse</b>	<b>all charged</b>	122.7	81.27	60.10	14.52	4.39
<b>Energy</b>	$N_{coll} * E_T^{pA}$	121.8	84.33	59.74	11.50	
<b>(GeV)</b>	$N_{proj} * E_T^{pA}$	80.90	50.22	36.17	7.6	
<b>Mean Transverse</b>	<b>all neutrals</b>	89.87	59.43	44.10	10.64	3.15
<b>Energy</b>	$N_{coll} * E_T^{pA}$	87.41	60.1	42.87	8.25	
<b>(GeV)</b>	$N_{proj} * E_T^{pA}$	58.05	36.03	25.95	5.44	

TABLE IV. Comparison of average multiplicities calculated in C - Air collisions at different energies with the expectation in two different superposition models.  $N_p$  is the average number of projectile nucleons taking part in the inelastic C - Air collision. The energies given are the energy per nucleon.

ENERGY TeV	$N_p$	$n_{\pi^+}^{C-Air}$	$n_{\pi^+}^{p-Air}$	$n_{\pi^+}^{p-p}$	$N_p n_{\pi^+}^{p-p}$	$N_p n_{\pi^+}^{p-Air}$
1	2.23	8.20	2.24	4.89	10.90	4.99
10	2.40	13.96	3.77	7.27	17.44	9.05
100	2.66	27.11	6.70	10.78	28.67	17.82
1000	2.93	47.33	11.58	16.16	47.34	33.92
10000	3.44	101.70	22.65	27.00	92.88	77.92

TABLE V. Comparison of  $Z_\pi$  spectrum weighted moments calculated in C - Air collisions at different energies with the expectation in two different superposition models.  $N_p$  is the average number of projectile nucleons taking part in the inelastic C - Air collision. The energies given are the energy per nucleon.

ENERGY TeV	$N_p$	$Z_{\pi^+}^{C-Air}$	$Z_{\pi^+}^{p-Air}$	$Z_{\pi^+}^{p-p}$	$N_p Z_{\pi^+}^{p-p}$	$N_p Z_{\pi^+}^{p-Air}$
1	2.23	0.047	0.010	0.026	0.057	0.022
10	2.40	0.047	0.012	0.024	0.058	0.029
100	2.66	0.049	0.010	0.023	0.061	0.027
1000	2.93	0.054	0.011	0.028	0.082	0.032
10000	3.44	0.062	0.012	0.024	0.082	0.041

TABLE VI. Inelasticities in p - Air collisions as calculated with HIJING model

ENERGY TeV	$K_{\pi^+}$	$K_{\pi^-}$	$K_{\pi^0}$	$K_{K^+}$	$K_{K^-}$	$K_{ch}$	$K_{neu}$	$K_{all}$
1	0.053	0.045	0.052	0.0076	0.0070	0.227	0.138	0.366
10	0.056	0.047	0.054	0.0080	0.0070	0.240	0.150	0.390
100	0.060	0.052	0.060	0.0092	0.0080	0.271	0.165	0.435
1000	0.068	0.059	0.066	0.0100	0.0100	0.289	0.183	0.472
10000	0.080	0.072	0.082	0.0126	0.0123	0.306	0.215	0.522

TABLE VII. Comparison of  $Z_{\pi}$  and  $Z_K$  moments calculated in p - Air collisions at different energies with the expectation in different models : HIJING, DPMJET [4], [5], HEMAS [21] and SIBYLL , [22].

	HIJ	DPM	HEMAS	SIBYLL	HIJ	DPM	HEMAS	SIBYLL
ENERGY TeV	$Z_{\pi}$	$Z_{\pi}$	$Z_{\pi}$	$Z_{\pi}$	$Z_K$	$Z_K$	$Z_K$	$Z_K$
1	0.046	0.067	0.061	0.072	0.0080	0.0098	0.0104	0.0073
10	0.043	0.069	0.057	0.068	0.0071	0.0099	0.0113	0.0071
100	0.040	0.068	0.056	0.067	0.0066	0.0102	0.0116	0.0070
1000	0.040	0.066	0.056	0.066	0.0068	0.0101	0.0123	0.0070
10000	0.042				0.0076			



p + p (300 GeV) RAPIDITY AND TRANSVERSE MOMENTUM, HIJING

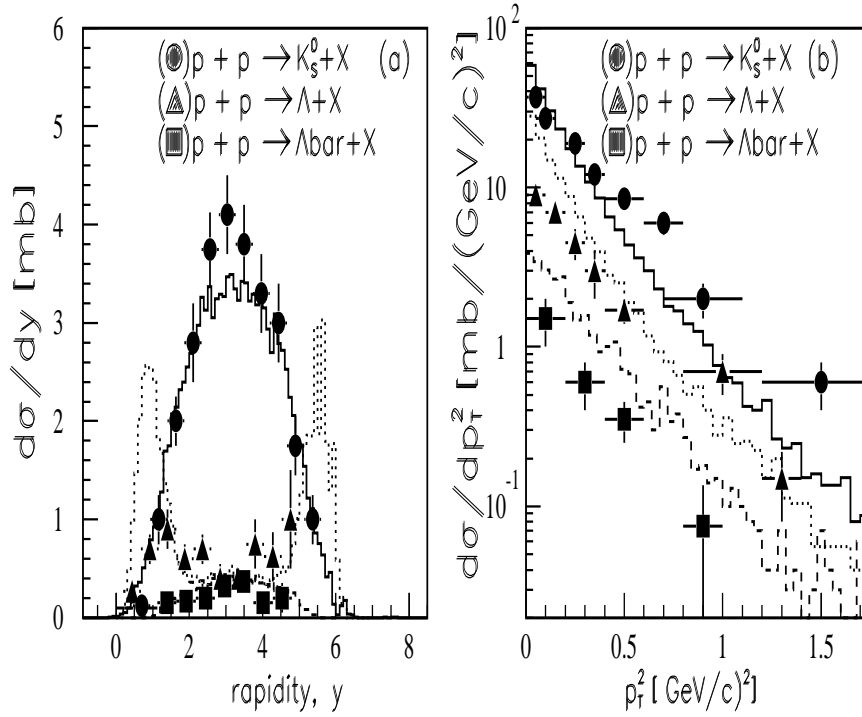


Figure 1

FIG. 1. Rapidity (Fig. 1a) and transverse momenta (Fig. 1b) distributions of  $\Lambda^0$  (dotted histograms),  $\bar{\Lambda}^0$  (dashed histograms), and  $K_S^0$  (full histograms) produced in  $pp$  interactions at 300 GeV. HIJING results are shown by histograms. The experimental data are taken from Lo Pinto et al. [53].

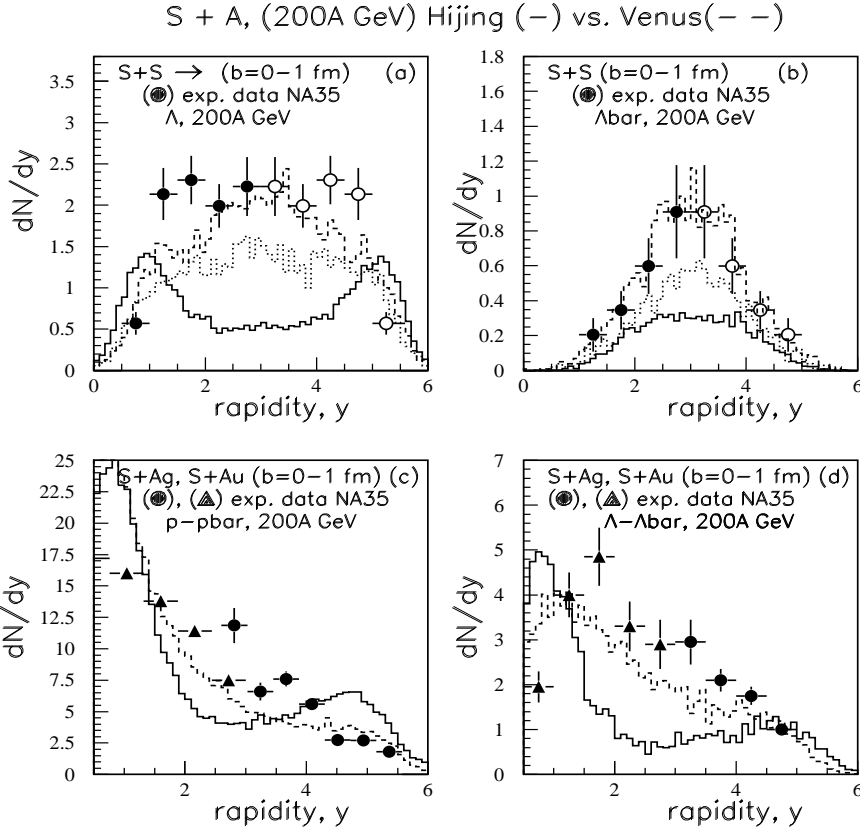


Figure 2

FIG. 2. Rapidity distributions of  $\Lambda$  and  $\bar{\Lambda}$  produced in central SS collisions at 200A GeV (Fig. 2a and Fig. 2b) respectively. In parts (b) the  $p - \bar{p}$  distributions are shown while parts (d) correspond to the  $\Lambda - \bar{\Lambda}$  distributions for S + Ag, S + Au interactions at 200A GeV. Expectations based on HIJING model are depicted as solid histograms. The theoretical predictions based on VENUS model are depicted as dotted histograms (option without final state interaction) and as dashed histograms (option including final state interactions). The NA35 data (full circles) are from Alber et al. [39] for part (a) and (b) and from Rörich et al. [29] for part (c) and (d). The open circles show the distributions for SS collisions reflected at midrapidity.

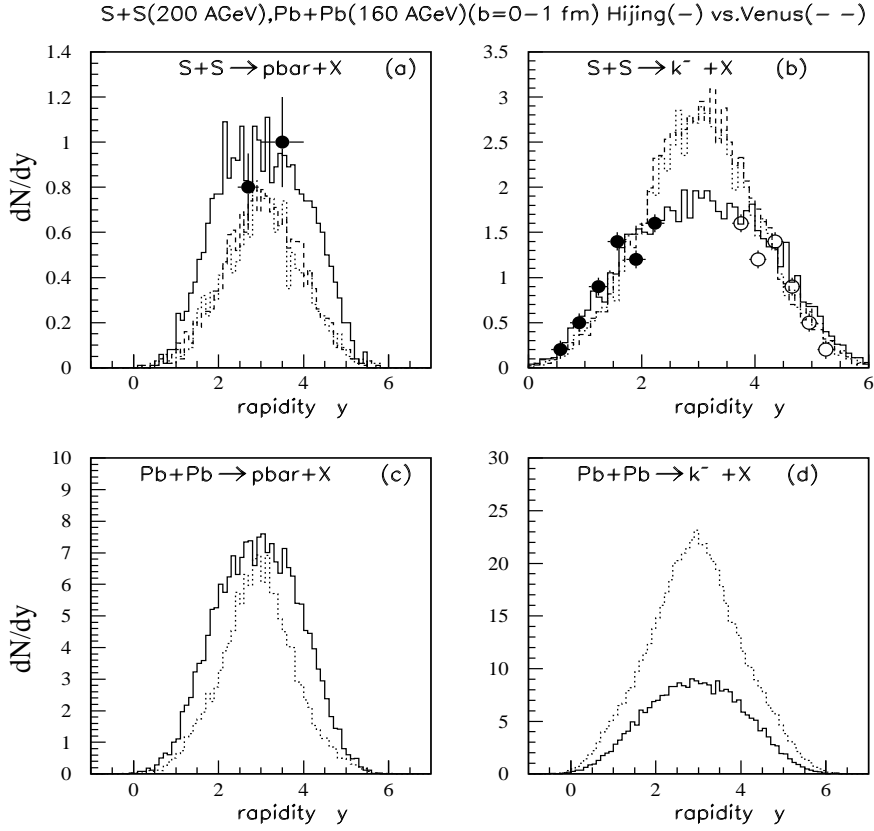


Figure 3

FIG. 3. Comparison of central  $S + S$  collisions at 200 AGeV (Fig. 3a -antiproton and Fig. 3b - negative kaons) with central  $PbPb$  collisions at 160 AGeV (Fig. 3c-antiproton and Fig. 3d- negative kaons). The experimental data are from NA44 [?] for antiprotons and from NA35 [41] for negative kaons. The open circles show the distributions for SS collisions reflected at mid-rapidity. The solid, dashed and dotted histograms have the same meaning as in Fig. 2.

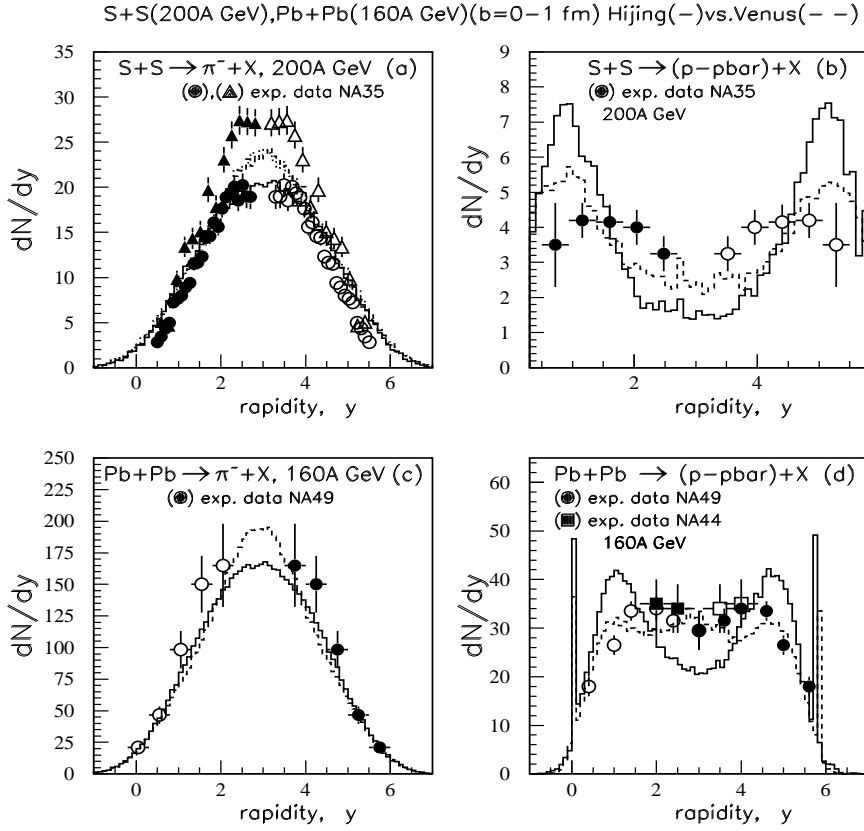


Figure 4

FIG. 4. Comparison of central  $S + S$  at 200 AGeV (a,b) NA35 [29,38] and central  $Pb + Pb$  at 160 AGeV (c,d) (NA49 [30,32,36] (solid circles), NA44 [31](solid squares)) data with calculations. Open circles and open squares are reflected data around mid-rapidity. Solid and dashed histograms correspond to HIJING and VENUS models respectively.

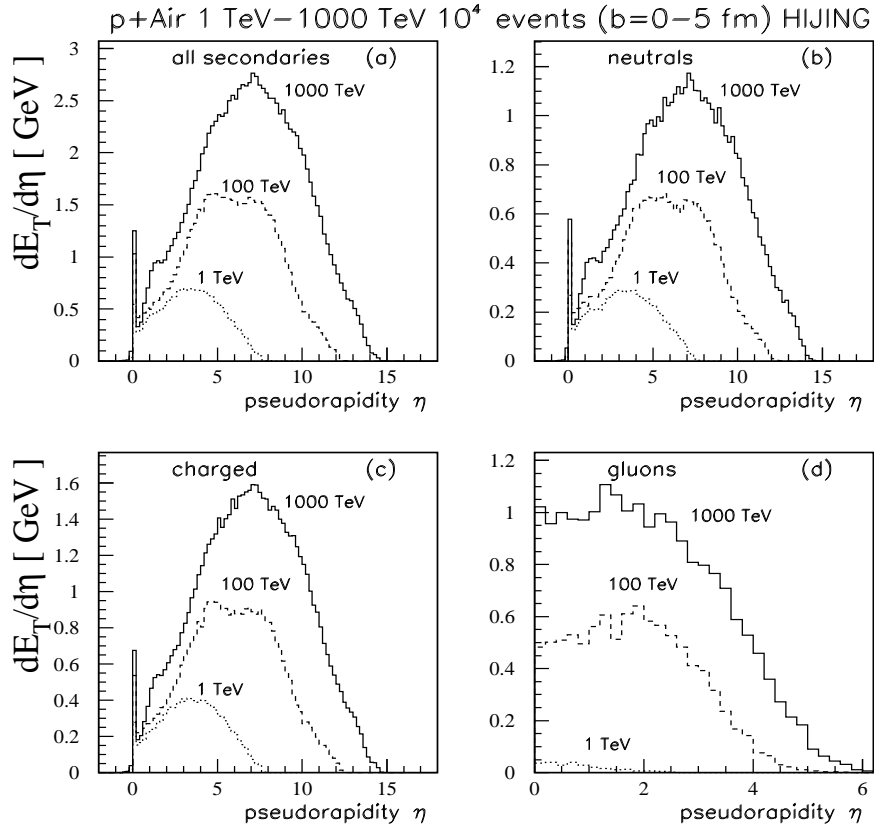


Figure 5

FIG. 5. Pseudorapidity distributions for transverse energy of secondary produced particles: all secondaries (Fig. 5a) , all neutrals( Fig. 5b) , all charged (Fig. 5c) and gluons (Fig. 5d) in  $p + Air$  Nucleus interactions . The dotted(for 1 TeV laboratory energy), dashed(for 100 TeV laboratory energy) and solid (for 1000 TeV laboratory energy) histograms are theoretical values given by HIJING model.

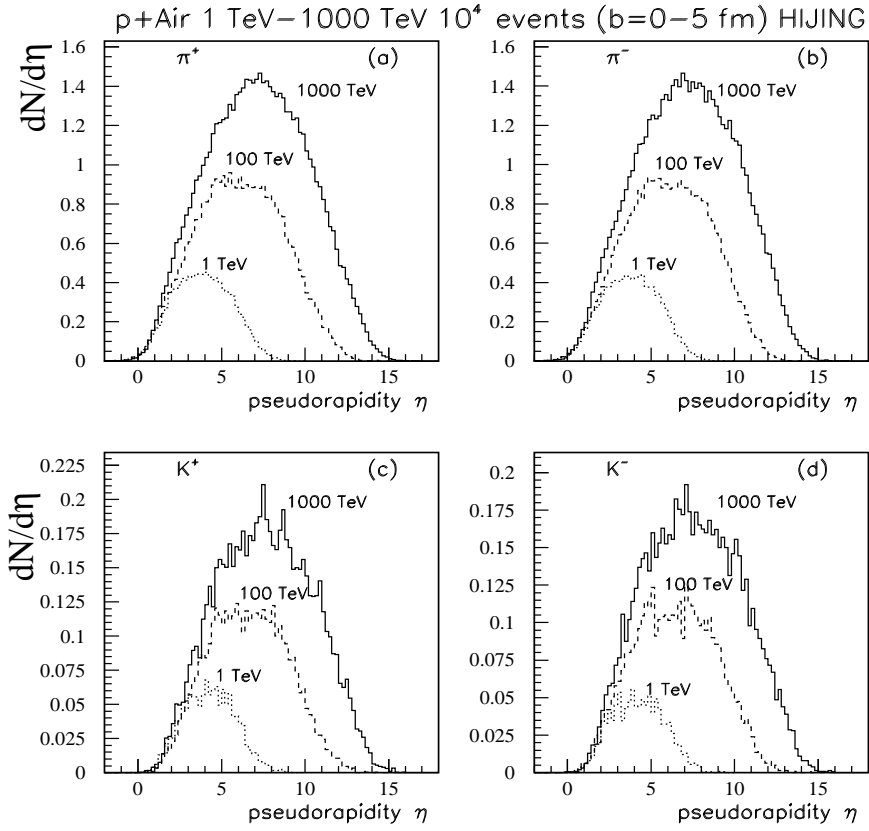


Figure 6

FIG. 6. Pseudorapidity distributions for  $p + \text{Air} \rightarrow \pi^+ + X$  (Fig. 6a),  $p + \text{Air} \rightarrow \pi^- + X$  (Fig. 6b),  $p + \text{Air} \rightarrow K^+ + X$  (Fig. 6c),  $p + \text{Air} \rightarrow K^- + X$  (Fig. 6d), at 1 TeV, 100 TeV and 1000 TeV. The dotted, dashed and solid histograms have the same meaning as in Figure 5.

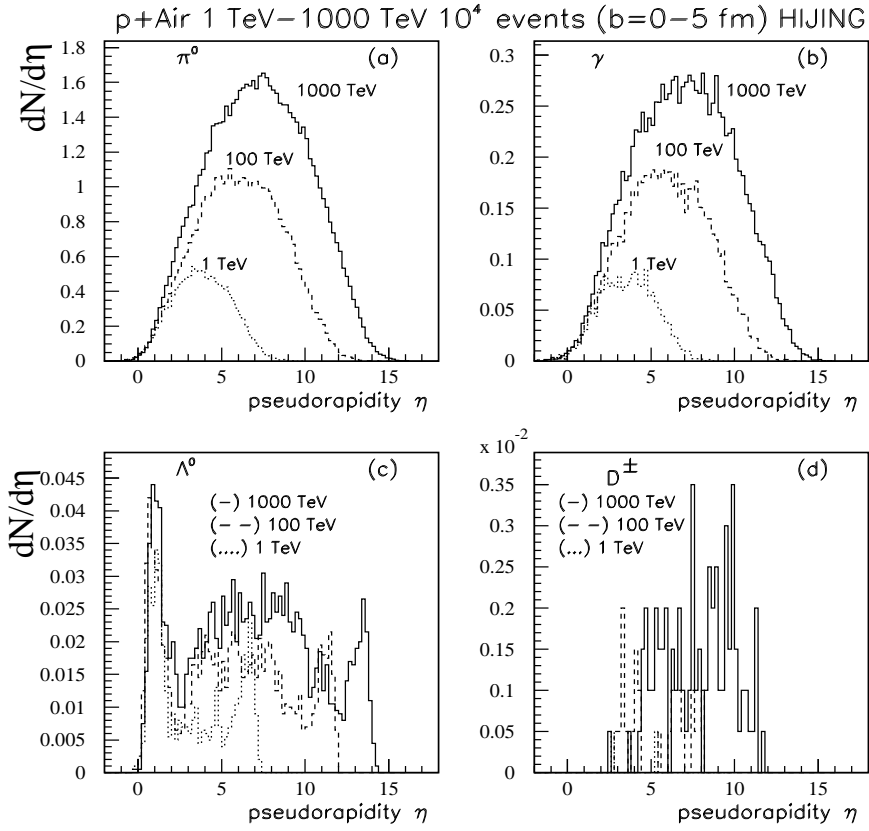


Figure 7

FIG. 7. Pseudorapidity distributions for  $p + Air \rightarrow \pi^0 + X$  (Fig. 7a),  $p + Air \rightarrow \gamma + X$  (Fig. 7b),  $p + Air \rightarrow \Lambda^0 + X$  (Fig. 7c),  $p + Air \rightarrow D^\pm + X$  (Fig. 7d), at 1 TeV, 100 TeV and 1000 TeV. The dotted, dashed and solid histograms have the same meaning as in Figure 5.

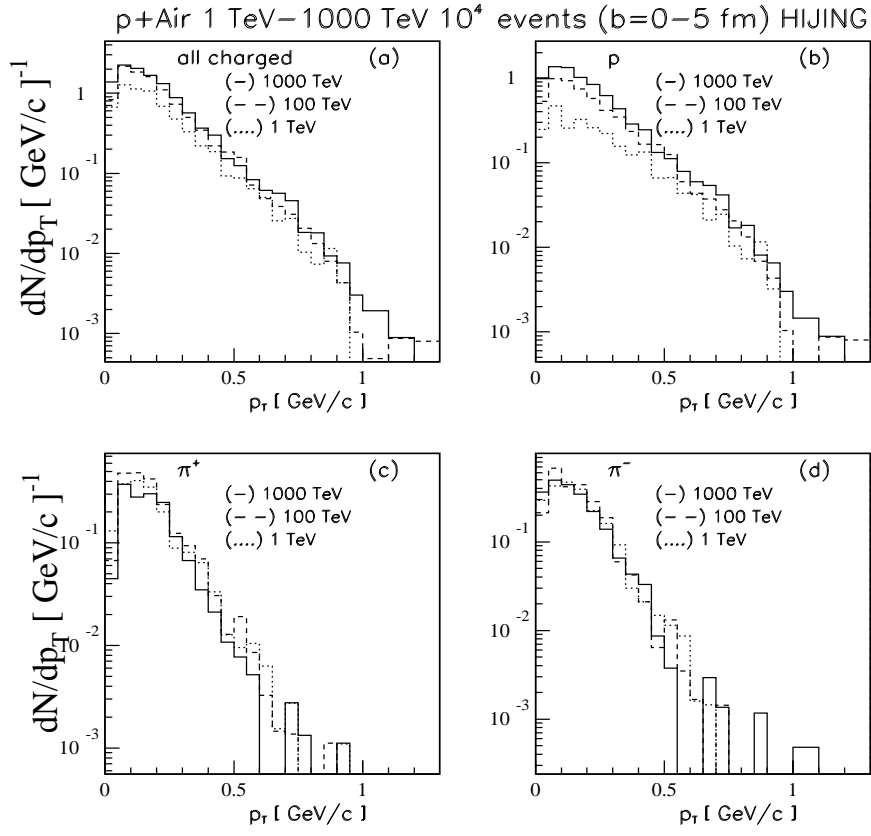


Figure 8

FIG. 8. Transverse momenta distributions for  $p + Air \rightarrow all\ charged + X$  (Fig. 8a),  $p + Air \rightarrow p + X$  (Fig. 8b),  $p + Air \rightarrow \pi^+ + X$  (Fig. 8c),  $p + Air \rightarrow \pi^- + X$  (Fig. 8d), at 1 TeV, 100 TeV and 1000 TeV. The dotted, dashed and solid histograms have the same meaning as in Figure 5.



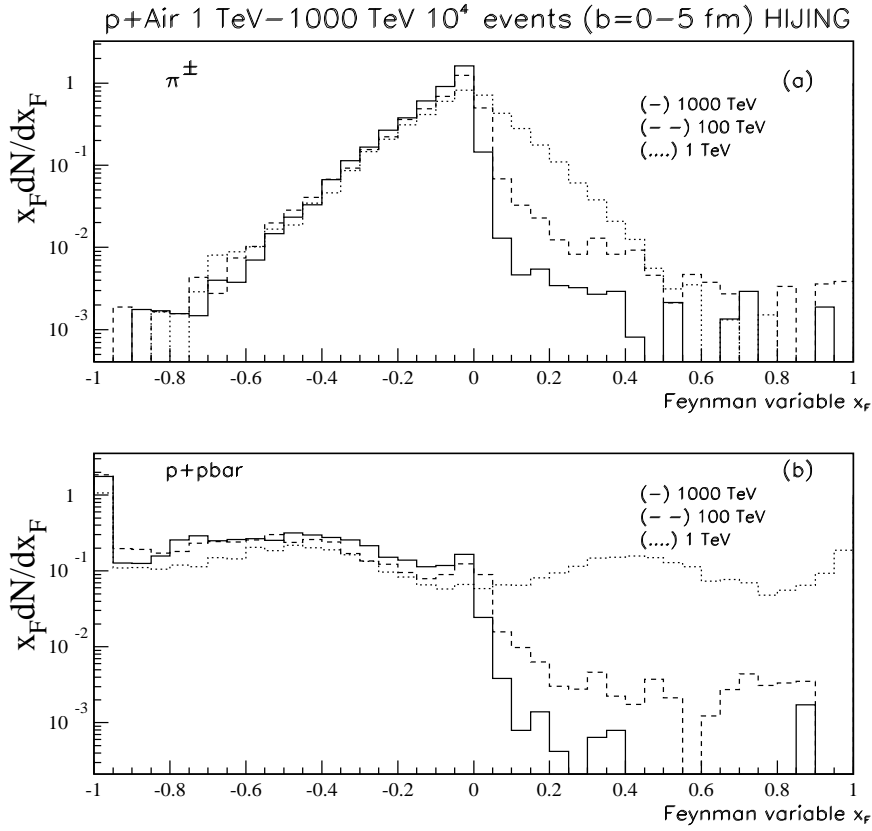


Figure 9

FIG. 9. Test of Feynman scaling in the production of  $p + Air \rightarrow \pi^\pm + X$  collisions (Fig. 9a) and  $p + Air \rightarrow p + \bar{p} + X$  collisions (Fig. 9b), between 1 TeV - 1000 TeV. The Feynman  $-x_F$  distributions were calculated with HIJING model. The dotted, dashed and solid histograms have the same meaning as in Figure 5.

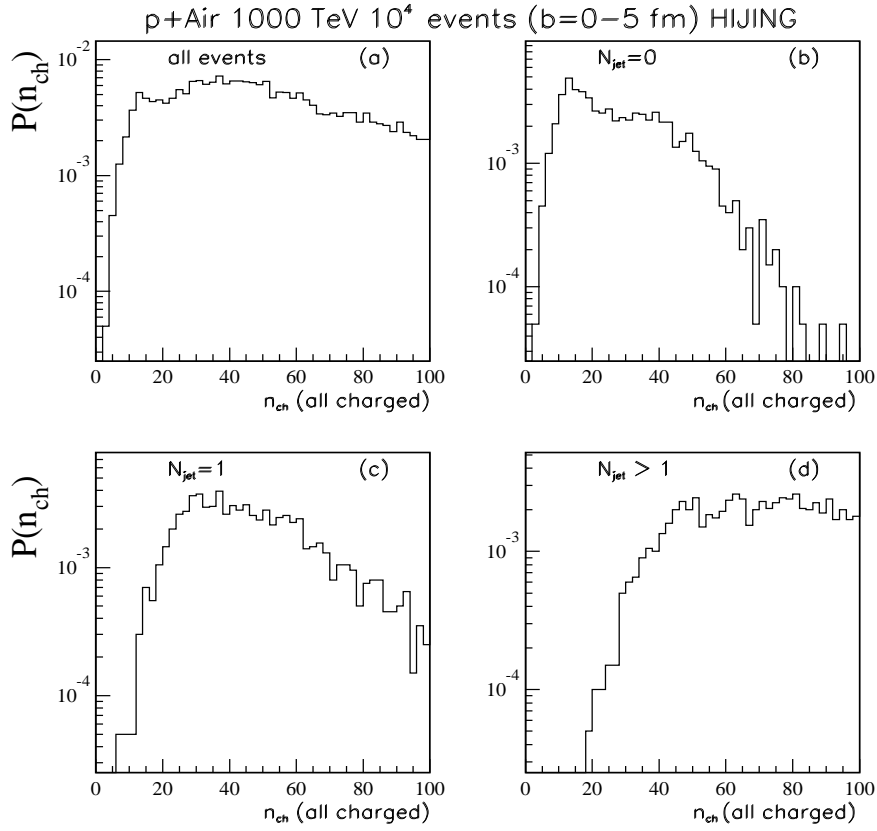


Figure 10

FIG. 10. Charged multiplicities distributions in  $p + Air$  interactions at 1000 TeV. Contributions from all events are depicted in Fig. 10a. In Fig. 10b the histogram is from HIJING model calculations with contributions from events with  $N_{jet} = 0$ , Fig. 10c the histogram is from calculations with contributions from events with  $N_{jet} = 1$  and in Fig. 10d the histogram is from calculations with contributions from events with  $N_{jet} > 1$ .

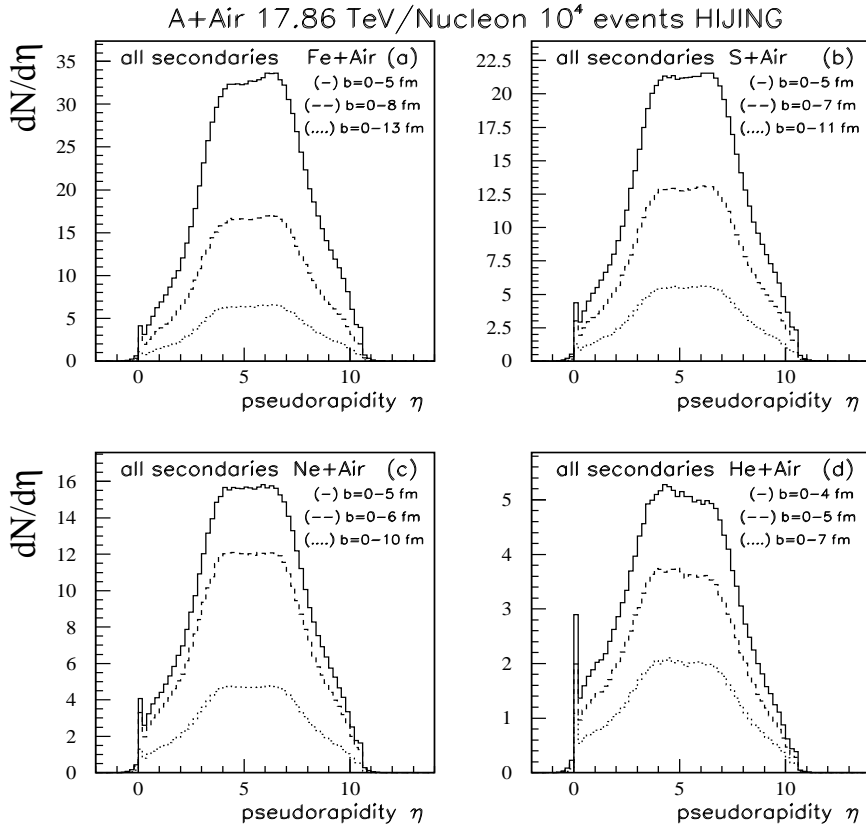


Figure 11

FIG. 11. Pseudorapidity distributions for all secondaries produced in Fe+Air interactions(Fig. 11a),S+Air interactions(Fig. 11b), Ne+Air interactions(Fig. 11c)and He+Air interactions (Fig. 11d) at 17.86 TeV/Nucleon for events generated in different impact parameters intervals ( $b_{min}, b_{max}$ ). See the text for explanations.

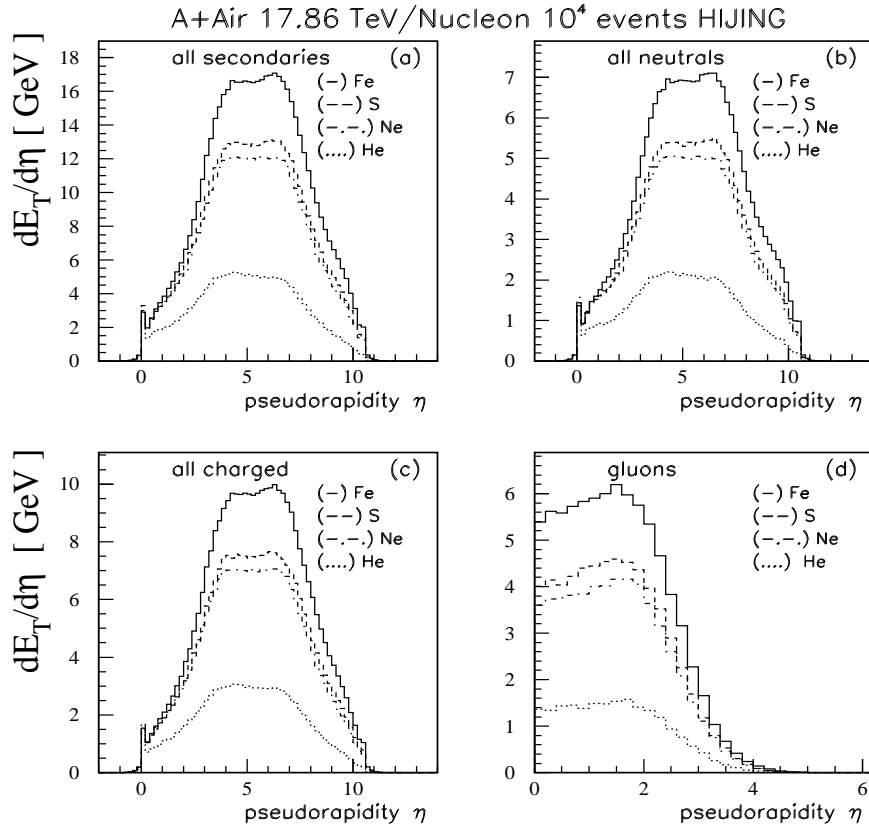


Figure 12

FIG. 12. Pseudorapidity distributions for transverse energy of secondary produced particles :all secondaries (Fig. 12a) ; all neutrals (Fig. 12b) ; all charged (Fig. 12c) ; gluons (Fig. 12d) in  $A + Air$  interactions at 17.86 TeV/Nucleon. The theoretical values were calculated with HIJING model and are depicted by dotted (He+Air) ; dot-dashed (Ne+Air) ; dashed (S+Air) and solid (Fe+Air) histograms.

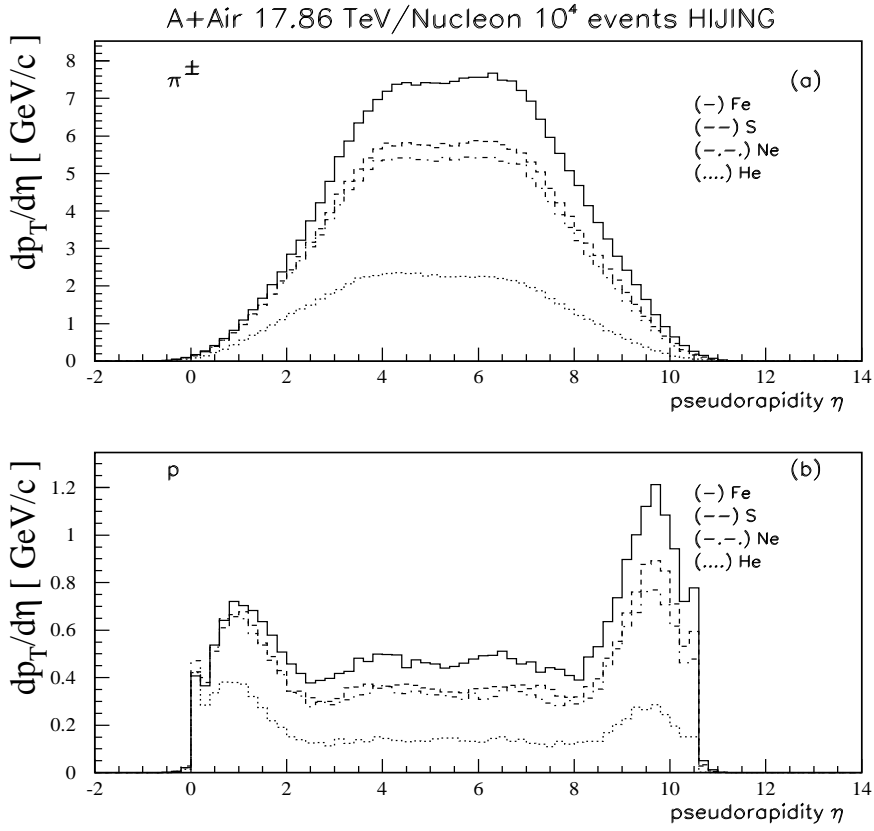


Figure 13

FIG. 13. Pseudorapidity distributions for transverse momenta of secondary particles for  $A + Air \rightarrow \pi^\pm + X$  (Fig. 13a) and  $A + Air \rightarrow p + X$  collisions (Fig. 13b) at 17.86 TeV/Nucleon. The histograms have the same meaning as in Figure 12.

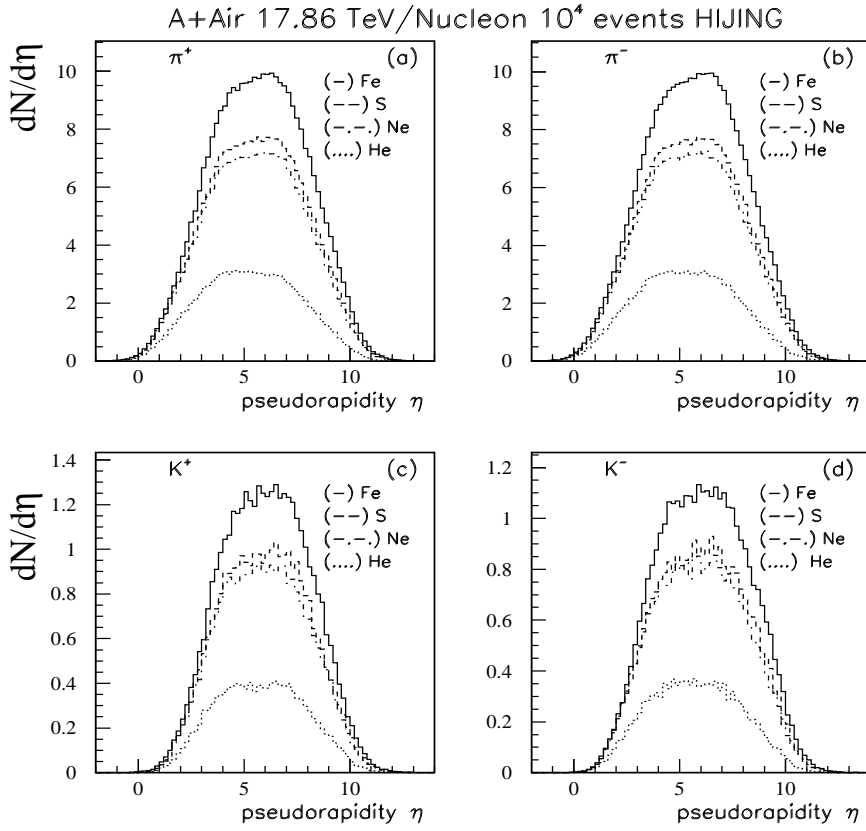


Figure 14

FIG. 14. Pseudorapidity distributions for  $A + Air \rightarrow \pi^+ + X$  (Fig. 14a),  $A + Air \rightarrow \pi^- + X$  (Fig. 14b),  $A + Air \rightarrow K^+ + X$  (Fig. 14c),  $A + Air \rightarrow K^- + X$  (Fig. 14d), at 17.86 TeV/Nucleon. The histograms have the same meaning as in Figure 12.

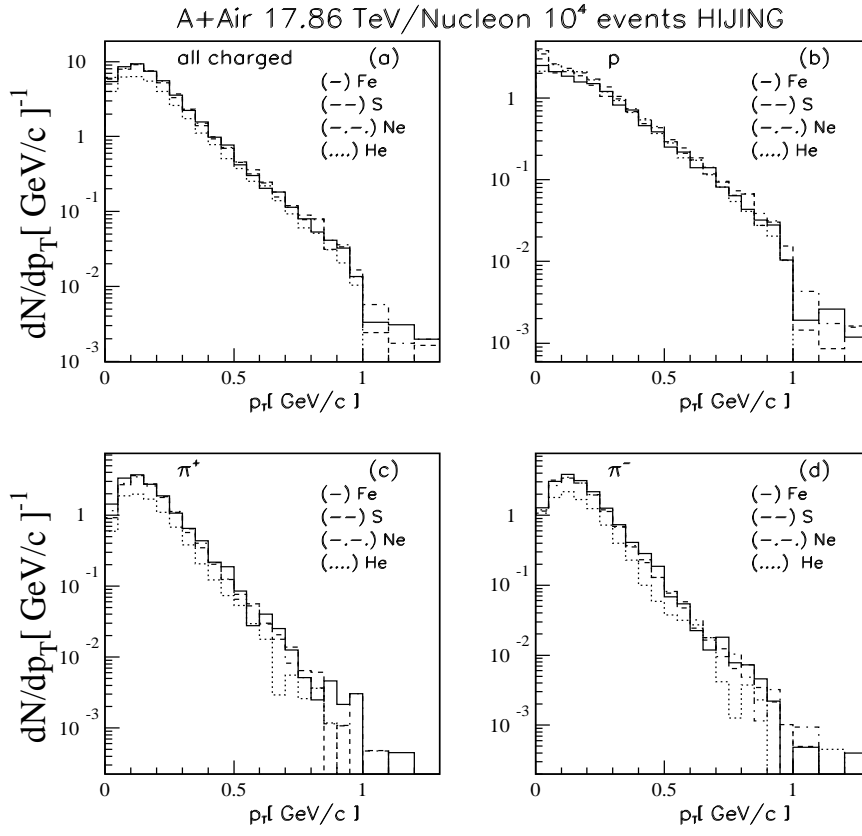


Figure 15

FIG. 15. Transverse momenta distributions for  $A + Air \rightarrow all\ charged + X$  (Fig. 15a),  $A + Air \rightarrow p + X$  (Fig. 15b),  $A + Air \rightarrow \pi^+ + X$  (Fig. 15c),  $A + Air \rightarrow \pi^- + X$  (Fig. 15d), at 17.86 TeV/Nucleon. The histograms have the same meaning as in Figure 12.

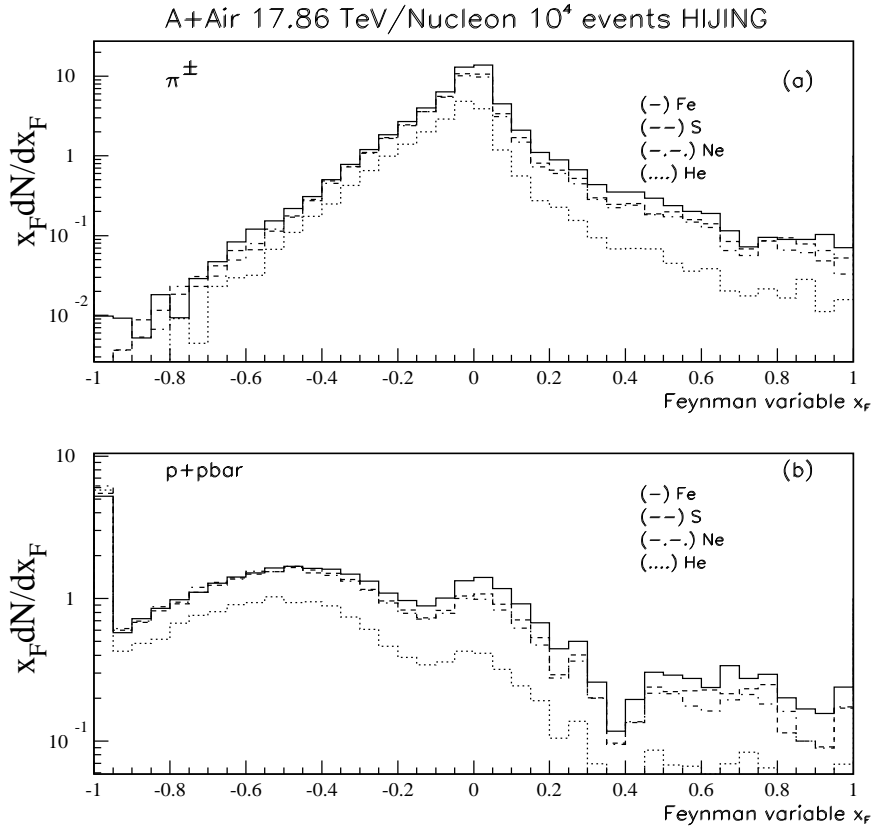


Figure 16

FIG. 16. The Feynman  $x_F$  distributions in the production of  $A + Air \rightarrow \pi^\pm + X$  collisions (Fig. 16a) and  $A + Air \rightarrow p + \bar{p} + X$  collisions (Fig. 16b), at 17.86 TeV/Nucleon. The histograms have the same meaning as in Figure 12 .



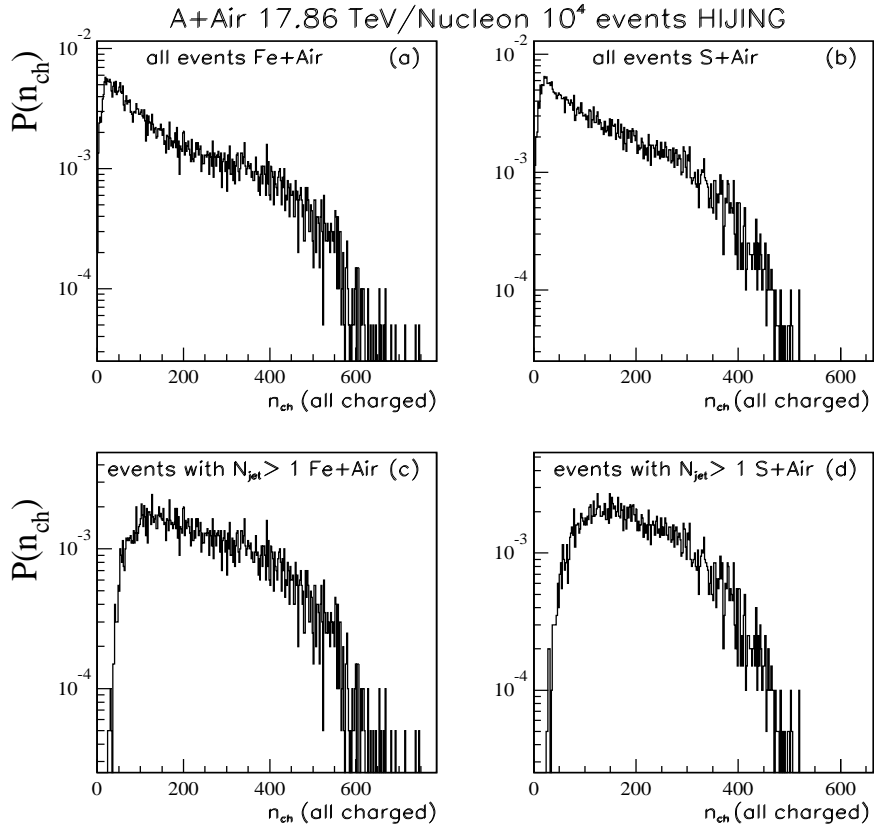


Figure 17

FIG. 17. Charged particles multiplicities distributions in Fe+Air interactions (Fig. 17a) and S+Air interactions (Fig. 17b) at 17.86 TeV/Nucleon. Contributions from events with number of minijets  $N_{\text{jet}} > 1$  are represented in Fig. 17c for Fe+Air interactions and in Fig. 17d for S+Air interactions.

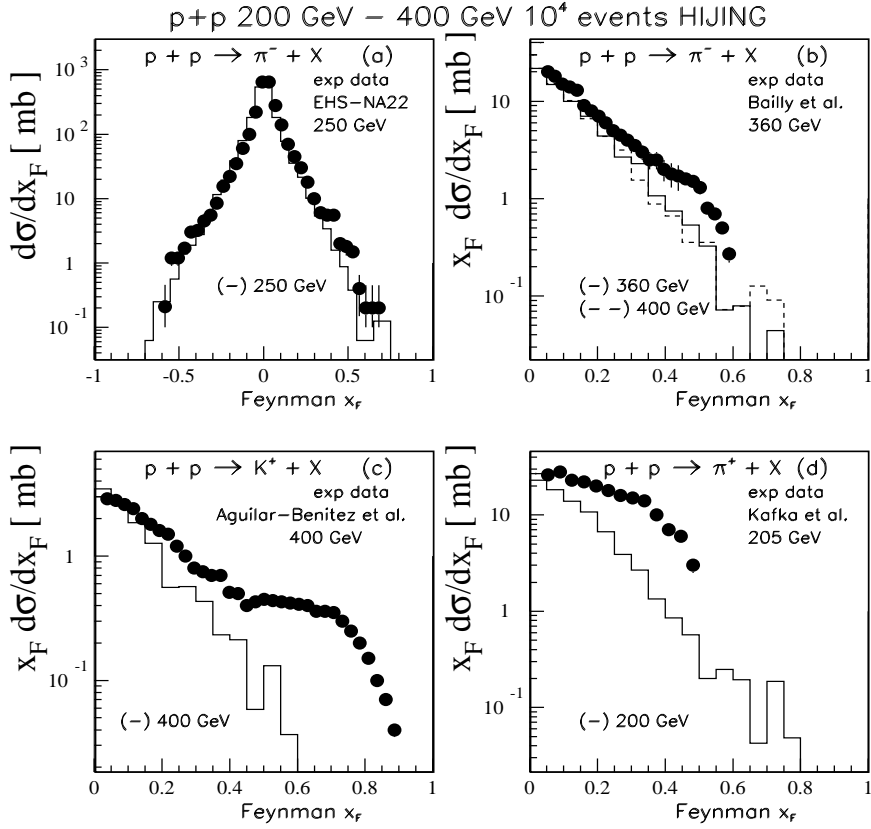


Figure 18

FIG. 18. Comparison of Feynman -  $x_F$  distributions of  $\pi^-$  mesons produced in proton - proton collisions at 250 GeV ( Fig. 18a).The experimental data are from the EHS - NA22 Collaboration [54] ; for proton - proton collisions at 360 GeV (Fig. 18b) .The experimental data are from Bailly et al. [55,59].The histogram are theoretical predictions for 360 GeV (dashed) and for 400 GeV (solid) . Comparison of Feynman -  $x_F$  distributions of  $K^+$  - mesons produced in proton - proton collision at 400 GeV (Fig. 18c).The experimental data are from LEBC - EHS Collaboration [56] ; Comparison of Feynman -  $x_F$  distributions of  $\pi^+$  - mesons produced in proton - proton collision at 205 GeV (Fig. 18d). The experimental data are from Kafka et al. [57].

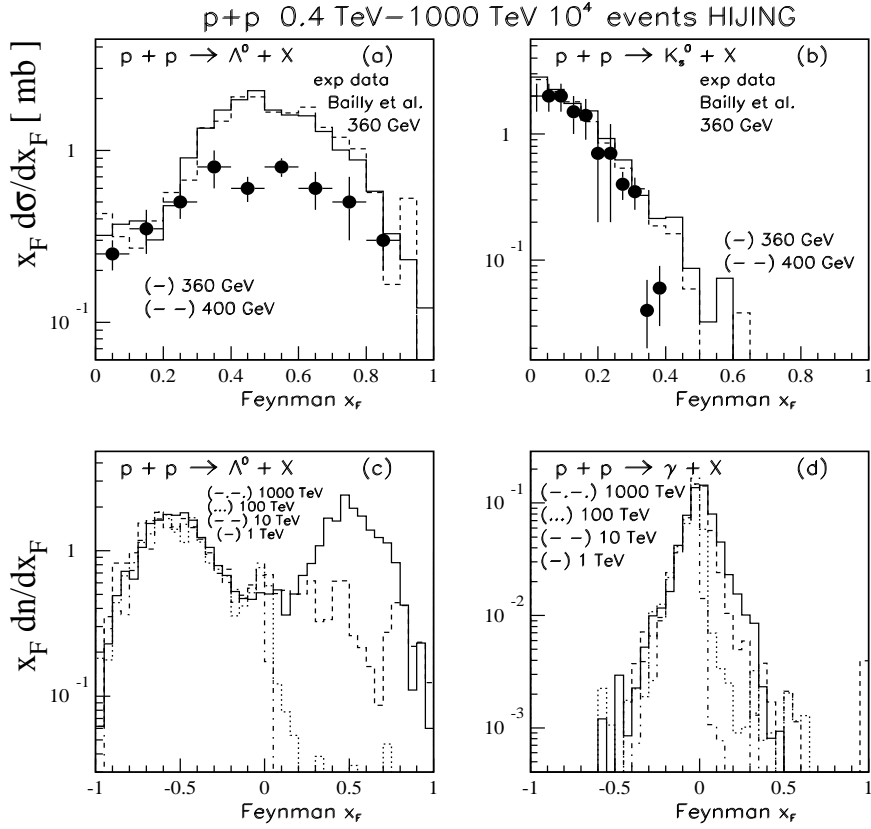


Figure 19

FIG. 19. Comparison of Feynman  $x_F$  distributions of  $\Lambda^0$  (Fig. 19a) and  $K_s^0$  (Fig. 19b) produced in proton - proton collisions at 360 GeV . The histogram are theoretical predictions for 360 GeV (dashed) and for 400 GeV (solid). The experimental data are from Bailly et al. [55]. Feynman  $x_F$  distributions of  $\Lambda^0$  (Fig. 19c) and  $\gamma$  (Fig. 19d) in energy region 1 TeV - 1000 TeV. The histograms are HIJING model predictions for 1 TeV (solid), 10 TeV (dashed), 100 TeV (dotted) and 1000 TeV (dot dashed).

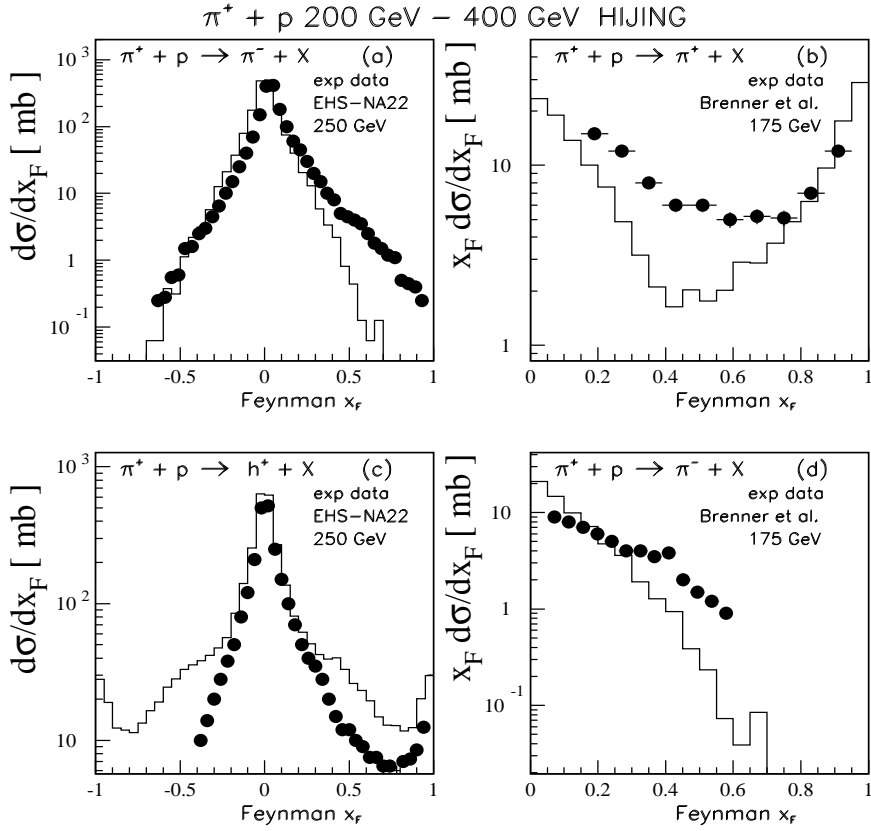


Figure 20

FIG. 20. Comparison of Feynman  $x_F$  distributions of  $\pi^-$  - mesons produced in  $\pi^+ + p$  collisions at 250 GeV (Fig. 20a). The experimental data are from the EHS - NA22 Collaboration [54] ;  $\pi^+$  - mesons produced in  $\pi^+ + p$  collisions at 250 GeV (Fig. 20b). The experimental data are from Brenner et al. [58]. Comparison of Feynman  $x_F$  distributions of positives charged  $h^+$  produced in  $\pi^+ + p$  collisions at 250 GeV (Fig. 20c). The experimental data are from the EHS - NA22 Collaboration [54]. Comparison of Feynman  $x_F$  distributions of  $\pi^-$  - mesons produced in  $\pi^+ + p$  collisions at 175 GeV (Fig. 20d) . The experimental data are from Brenner et al. [58].